The main geological factors controlling the Wufeng-Longmaxi shale gas content

Yijun Zheng, Yuhong Liao, Yunpeng Wang, Yongqiang Xiong, and Ping'an Peng

ABSTRACT

Changning and Fuling are two of the best-known shale gas fields in China, located at two different depositional centers of the Upper Ordovician Wufeng Formation to the lower Silurian Longmaxi Formation in the Sichuan Basin. However, there are significant differences in the gas content of the Wufeng-Longmaxi shales between these two areas, despite their similar average total organic carbon contents and thickness. To elucidate the main factors responsible for the differences in the shale gas content between Changning and Fuling, two shallow wells were drilled to investigate their mineralogical and petrophysical properties as well as the organic matter–associated pore structure of the Wufeng-Longmaxi shales. A comparison of these reservoir properties was also made with those of the Jiaoye 4 well from the Fuling shale gas field. Because the Wufeng-Longmaxi shales in these two areas were deposited within different sedimentary environments and experienced different tectonic intensities, the present study focused mainly on investigating whether and how these differences have affected the petrophysical properties of the shale interval. The results indicated that intensive carbonate cementation in Changning significantly reduced the total pore volume and total specific surface area of the shale interval, and thus degraded the reservoir connectivity. However, compared with the Fuling field, a relatively weak tectonic compaction deformation in the Changning field was beneficial to the preservation of pore volume. Therefore, more intensive carbonate cementation may have been one critical geological factor responsible for the lower gas content in the Wufeng-Longmaxi shale reservoirs in the southern Sichuan Basin.

Manuscript received October 28, 2018; provisional acceptance October 1, 2019; revised manuscript received November 1, 2019; revised provisional acceptance January 7, 2021; 2nd revised manuscript received January 16, 2021; 2nd revised provisional acceptance February 25, 2021; 3rd revised manuscript received April 30, 2021; 3rd revised provisional acceptance October 14, 2021; 4th revised manuscript received October 18, 2021; final acceptance October 29, 2022.
DOI:10.1306/07132218243

AUTHORS

YIJUN ZHENG ~ *State Key Laboratory of Organic Geochemistry, Guangzhou Institute of Geochemistry, Chinese Academy of Sciences (CAS), Guangzhou, People's Republic of China; CAS Center for Excellence in Deep Earth Science, Guangzhou, People's Republic of China; zhengyijun@gig.ac.cn, zyjln123@sina.com*

Yijun Zheng is currently a postdoctoral scholar at the State Key Laboratory of Organic Geochemistry, Guangzhou Institute of Geochemistry, CAS. He earned his B.S. degree and Ph.D. from Chengdu University of Technology and Guangzhou Institute of Geochemistry, CAS in 2011 and 2018, respectively. His research focuses on shale sedimentology, petrophysical properties of shale, and shale reservoir quality prediction.

YUHONG LIAO ~ *State Key Laboratory of Organic Geochemistry, Guangzhou Institute of Geochemistry, CAS, Guangzhou, People's Republic of China; CAS Center for Excellence in Deep Earth Science, Guangzhou, People's Republic of China; liaoyh@gig.ac.cn*

Yuhong Liao is an organic geochemist and a research fellow of the Guangzhou Institute of Geochemistry, CAS. He earned his B.S. degree and Ph.D. from Peking University and Guangzhou Institute of Geochemistry, CAS in 2000 and 2006, respectively. He is currently working on petroleum reservoir geochemistry and unconventional oil and gas. He is the corresponding author of this article.

YUNPENG WANG ~ *State Key Laboratory of Organic Geochemistry, Guangzhou Institute of Geochemistry, CAS, Guangzhou, People's Republic of China; CAS Center for Excellence in Deep Earth Science, Guangzhou, People's Republic of China; wangyp@gig.ac.cn*

Yunpeng Wang earned his B.S. degree and Ph.D. from Lanzhou University and Guangzhou Institute of Geochemistry, CAS in 1990 and 1996, respectively. He is currently working on gas geochemistry and petroleum system modeling relating to unconventional and deep gases. He is a member of the

International Scientific Committee of the International Conference on Gas Geochemistry.

YONGQIANG XIONG ~ *State Key Laboratory of Organic Geochemistry, Guangzhou Institute of Geochemistry, CAS, Guangzhou, People's Republic of China; CAS Center for Excellence in Deep Earth Science, Guangzhou, People's Republic of China; xiongyq@gig.ac.cn*

Yongqiang Xiong received his Ph.D. in geochemistry from the Guangzhou Institute of Geochemistry, CAS, in 2001. His general research interest is oil and gas geochemistry. His present research is focused on the quantitative characterization of the source and maturity of highly mature hydrocarbons.

PING'AN PENG ~ *State Key Laboratory of Organic Geochemistry, Guangzhou Institute of Geochemistry, CAS, Guangzhou, People's Republic of China; CAS Center for Excellence in Deep Earth Science, Guangzhou, People's Republic of China; pinganp@gig.ac.cn*

Ping'an Peng is an organic geochemist and a research fellow at the Guangzhou Institute of Geochemistry, CAS. He earned his B.S. degree and Ph.D. from Zhejiang University and Institute of Geochemistry, CAS, respectively. He has worked in petroleum geochemistry for 38 years. In 2013, he was elected as an academician of CAS.

ACKNOWLEDGMENTS

This work was financially supported by the Special Fund for Strategic Priority Research Program of the Chinese Academy of Sciences (Grant No. XDB10010301 and Grant No. XDA14010103) and the State Key Laboratory of Organic Geochemistry (Grant No. 135TP201602). We are grateful to Xi'Nan Yang, Peng Wang, Hengchao Li, and Long He for assistance in well drilling, and Qing Zeng for the assistance in pretreatment and instrumental analysis. Previous AAPG Editor Robert K. Merrill is especially acknowledged for constructive suggestions and comments. The authors also thank three anonymous reviewers and Chunqing Jiang for their valuable comments that helped to greatly improve the content and quality of the paper.

INTRODUCTION

With the development and application of horizontal drilling and hydraulic fracturing technology, unconventional shale oil and gas exploration and development have achieved great success in North America (Curtis, 2002; Hao et al., 2013). With the rapid adoption of new drilling and completion technologies, China has become the third country to realize commercial exploitation of shale gas, after the United States and Canada (Zou et al., 2016b). At present, shale gas fields in China are distributed mainly in the Sichuan Basin and its adjacent areas (Wei et al., 2016; Zou et al., 2016a). Two depositional centers of the Wufeng (Ordovician) and Longmaxi (Silurian) Formations are located in the southern and eastern Sichuan Basin (Wang et al., 2015), both with thick, high-quality shales in the Wufeng and Longmaxi Formations (total organic carbon [*TOC*] ≥ 2.0 wt. %). Accordingly, two major shale gas fields have been discovered producing from the Wufeng and Longmaxi Formations in the southern and eastern Sichuan Basin, namely, the Changning (or Weiyuan-Changning) field and the Fuling field, with proven geological reserves of 0.16×10^{12} m^3 (5.65×10^{12} ft^3) (Zou et al., 2016a) and 0.60×10^{12} m^3 (21.19×10^{12} ft^3) (Liu, 2018), respectively. It is worth noting that the gas reserve density of the shale gas production interval differs between the Changning and Fuling fields, in the range of 2.4–5.5 m^3/t (84.8–194.2 ft^3/t) for the former and 4.7–7.2 m^3/t (166.0–254.3 ft^3/t) for the latter (Zou et al., 2016a). Moreover, there is a significant variation in the gas production from different locations of the Wufeng-Longmaxi shales. For example, the initial production of an average single horizontal well from the Fuling field (more than 30 wells) is 33.4×10^4 m^3/day (1179.5×10^4 ft^3/day) (Zou et al., 2016b), whereas the initial production of an average single horizontal well from the YS108 well area (more than 20 wells) and the N201 well area (more than 20 wells) in the Changning shale gas field is 21.2×10^4 m^3/day (749.7×10^4 ft^3/day) and 13.5×10^4 m^3/day (476.7×10^4 ft^3/day) (Zou et al., 2016a), respectively. Therefore, the heterogeneity of the high-quality shale intervals in the Changning shale gas field is very strong (Jia et al., 2017), and the initial test output is relatively low and uneven.

Due to the heterogeneity and fine-grain character of the shale reservoirs (Loucks et al., 2009; Chen et al., 2015), most of the recent research on gas shales has focused on the nanopore structure of the shales and their controlling factors (e.g., the depositional environments, organic content, types and maturity of organic matter [OM], mineralogy, diagenesis, and structural deformation) (Loucks et al., 2012; Loucks and Reed, 2014; Cao et al., 2015; Han et al., 2016; Ma et al., 2016; Liang et al., 2017; Zhao et al., 2017a, b; Zheng et al., 2018). In general, the transgressive systems tract and the highstand systems tract, to which

the Wufeng-Longmaxi Formations belong, commonly contain siliceous and carbonaceous shale with excellent OM type (types I and II), high *TOC* and gas content, abundant brittle minerals, and good petrophysical properties (Guo and Zhang, 2014; Chen et al., 2015; Liang et al., 2016; Zou et al., 2016a; Zheng et al., 2018). Statistical production results showed that Wufeng-Longmaxi shale gas production varies greatly in the Sichuan Basin (Zhao et al., 2016b; Zou et al., 2016a). Due to the differences in geological settings of different regions, geological factors potentially affecting shale gas reserves, such as diagenetic alteration and mechanical compaction, have attracted a great deal of attention in recent years (Loucks et al., 2012; Milliken et al., 2013; Han et al., 2016, 2017). For example, previous studies documented that both carbonate cementation and mechanical compaction can reduce and destroy interparticle pores in shale reservoirs (Loucks et al., 2012; Milliken et al., 2013; Han et al., 2016, 2017; Zhao et al., 2017a).

Typical diagenetic (mesogenetic) alteration of minerals usually occurred at depths greater than 2000 m (>6562 ft) and temperatures above 70°C (158°F) (Morad et al., 2000). These transitions are believed to affect the petrophysical properties of various kinds of reservoirs. Diagenetic alterations of sandstones usually include the following: (1) the dissolution of the feldspar and carbonates (high-Mg calcite, aragonite, and nonferroan carbonate cement) and (2) the reprecipitation of quartz and carbonate cement (Ma et al., 2017). Based on optical micrographs and scanning electron microscopy (SEM) images, the observed dissolution pores of metastable minerals have been linked to the release of organic acids and CO_2 during the thermal maturation of OM (MacGowan and Surdam, 1990; Morad et al., 2010; Schieber, 2010; Ma et al., 2017). Carbonate cement (mostly calcite) is recognized as one of the most abundant diagenetic minerals, strongly modifying the petrophysical properties of sandstone reservoirs and affecting fluid flow during production (Dutton et al., 2002; Morad et al., 2010; Ma et al., 2017). A few studies (Schieber, 2010; Han et al., 2016, 2017; Zhao et al., 2017a) have been conducted on the connection between the carbonate content and shale reservoir properties. When the carbonate content is low (<10%), the carbonate grains are commonly scattered, and the effect of carbonates on the petrophysical property of shales can be ignored (Schieber, 2010). In contrast, abundant carbonate (10% or more) in shales may imply that the carbonate grains were reworked into thin laminae (Schieber, 2010). Based on the rock mineral compositions of the Wufeng-Longmaxi shales, Han et al. (2016) proposed that only low calcareous mixed shale with high *TOC* is good for exploration. Han et al. (2017) reported that the porosity of Jurassic (Toarcian) Posidonia Shale (Lower Saxony, Germany) was reduced from 14.03 vol. % at the immature stage to 4.05 vol. % in the oil-mature stage by cementation.

In addition, mechanical compaction also can affect shale reservoirs (Loucks et al., 2012; Zhao et al., 2017a). Mechanical compaction can be caused by the vertical stresses during burial and the lateral stresses during tectonic deformation (Gutierrez and Wangen, 2005; Obradors-Prats et al., 2017). In the early stage of burial, with the increase in overlying formation pressure, the pore volume of clastic mudstone was lost mainly through compaction (Bridge and Demicco, 2008; Loucks et al., 2012; Zhao et al., 2017a). A previous study by Curtis et al. (2012) suggested that the absence or paucity of OM pores in some mature shales may be attributed to the compaction after or during the formation of OM pores. Mechanical compaction, which is the most significant process in mudstone diagenesis (Choquette and Pray, 1970; Loucks et al., 2012), can result in the reduction of initial porosities of mudstones by 60% to 80% at the time of deposition (Bridge and Demicco, 2008). In addition to the pressure of overlying strata, shale can be affected by regional tectonic stresses. The Sichuan Basin and its adjacent areas have undergone multiple uplifting events and intense folding and thrusting processes (Hao et al., 2013; Guo and Zeng, 2015). Tectonic compaction deformation of different strata was proposed to have occurred through a northwest stepwise progression of deformation in southern China (Yan et al., 2003). The southern Sichuan Basin and its neighboring areas that are far away from the Qiyueshan thrust fault and characterized by low and gentle fault-fold belts may have experienced weaker tectonic deformation than the eastern Sichuan Basin, which is characterized by high and steep fault-fold belts (Yan et al., 2003; Jiang et al., 2015). Therefore, the relationship between shale pore structure development and the potential affecting factors, including carbonate cementation

and tectonic deformation, in different areas of the Sichuan Basin deserves further investigation.

Pore structure analysis of the shale reservoirs is the most important approach to evaluate the potential of shale gas resources (Chalmers et al., 2012; Loucks et al., 2012; Mastalerz et al., 2013; Milliken et al., 2013; Loucks and Reed, 2014; Zhao et al., 2017a; Zheng et al., 2018). A better understanding of the pore structure of the shale reservoirs is critical to the assessment of transportation and storage properties of shales and can provide guidance for shale gas exploration and development (Loucks et al., 2012; Kuila and Prasad, 2013; Han et al., 2016). Pore sizes have been divided into micropores (<2 nm), mesopores (2–50 nm), and macropores (>50 nm) (International Union of Pure and Applied Chemistry, Physical Chemistry Division, Commission on Colloid and Surface Chemistry, Subcommittee on Characterization of Porous Solids, 1994). To assess the pore features of the shale reservoirs, a range of quantitative and visual qualitative methods have been reported (Chalmers et al., 2012; Clarkson et al., 2012; Yang et al., 2016). The quantitative methods such as high-pressure Hg intrusion and low-pressure N_2 and CO_2 gas adsorption can be used to obtain information about porosity, specific surface area, pore volume, and pore size distribution of the studied shales (Chalmers et al., 2012; Mastalerz et al., 2013; Wei et al., 2016; Yang et al., 2016). Field emission–SEM (FE-SEM) images commonly provide a visual pore distribution and geometries in the shale reservoirs (Chalmers et al., 2012; Loucks et al., 2012; Milliken et al., 2013; Loucks and Reed, 2014; Han et al., 2016).

To achieve a better understanding of the main factors controlling pore volume and pore distribution of the organic-rich Wufeng-Longmaxi shale intervals, two shallow wells called Shuanghe-1 (SH-1, total depth of 157 m [~515 ft]) and Sanquan-1 (SQ-1, total depth of 91 m [~299 ft]), were drilled in the town of Shuanghe, Changning County, Sichuan Province, and the town of Sanquan, Nanchuan District of the Chongqing municipality, respectively, with their target formations being cored. The SH-1 well is in the Changning field and the SQ-1 well is near the Fuling field (Figure 1). The OM and mineralogy characterization, CO_2 and N_2 composited adsorption isotherms, Hg porosimetry, and FE-SEM imaging were performed on the cored shale samples of the two drilled wells as well as the Jiaoye 4 (JY 4) well (in the Fuling field) to investigate the complex pore structures and distributions and the interrelationships among different parameters of the shales. Based on these data, the effects of carbonate cementation and tectonic deformation on the petrophysical properties of the Wufeng-Longmaxi shales are discussed here. Our data provide not only an improved understanding of the main geological factors affecting the Wufeng-Longmaxi shale gas content between the Changning and Fuling fields but also the implications for the carbonate cementation to help constrain the optimal target for shale gas drilling and gas production worldwide.

GEOLOGIC SETTING

Several uplifts, including the Central Guizhou uplift and the Central Sichuan uplift, had formed in the Upper Yangtze platform by the Late Ordovician (Chen et al., 2015). During the Late Ordovician–early Silurian, the Sichuan Basin and its surrounding areas were characterized by an aerially extensive, low-energy, and anoxic sedimentary environment (Guo and Zhang, 2014; Chen et al., 2015). As a result, a succession of organic-rich black shale with abundant graptolites was deposited as the Upper Ordovician Wufeng Formation and the lower Silurian Longmaxi Formation (Luo et al., 2016; Ma et al., 2016; Zhao et al., 2017a).

The deposits in the Central Guizhou uplift consisted mainly of thick marine carbonates before the Silurian (Han et al., 2016; Zhao et al., 2017a). These carbonate deposits had been uplifted and eroded to some extent, and the dissolved carbonate minerals were believed to be one of the sources for carbonate in the shales deposited in the southern Sichuan Basin during the Late Ordovician–early Silurian (Han et al., 2016). Based on data from 37 geological sections and 18 exploratory wells in the Sichuan Basin and its neighboring areas, the carbonate contents of the Wufeng-Longmaxi shales in region I (Figure 1), where the Changning field is located, are in the range of 10% to 25% (Wang et al., 2015). In contrast, the average calcite content of the Jiaoye 1 (JY 1) well in region II, where the Fuling field is located, is only 3.8% (Guo and Zhang, 2014; Guo et al., 2014). The shallow well SH-1 was drilled in region I, whereas the SQ-1 well was drilled in region II (Figure 1A),

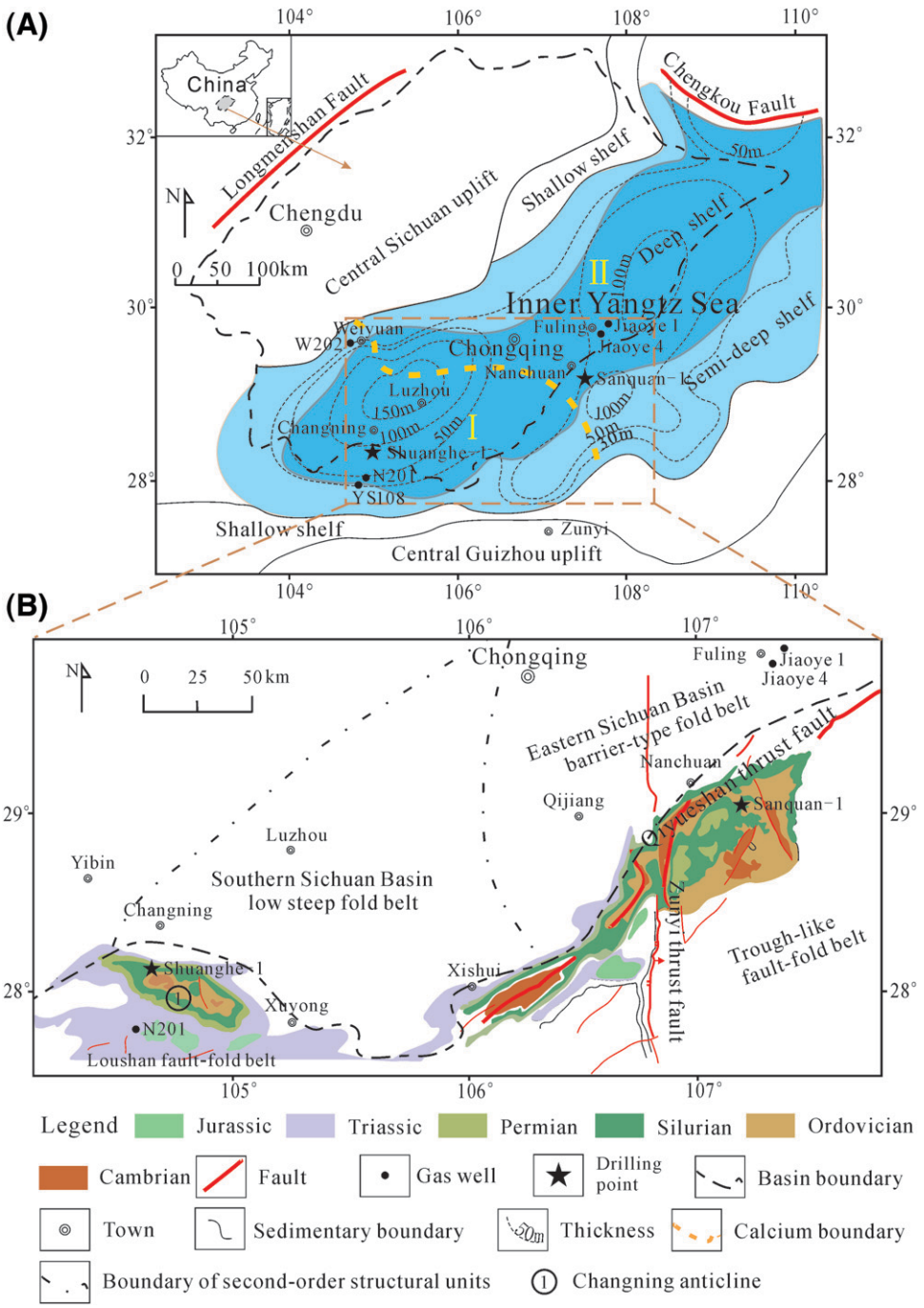

Figure 1. (A) Paleogeographic map of the Sichuan Basin and neighboring areas during the early Silurian (modified from Wang et al., 2015; Zheng et al., 2018). The calcium boundary divides the basin into region I for the calcareous shale (carbonate ≥10%) and region II for the less calcareous shale (carbonate <10%). (B) Regional, geological, and structural profiles of the studied areas. Locations of the samples/wells (e.g., Shuanghe-1, Sanquan-1) used in this study are also shown.

both having penetrated the lower part of the Longmaxi Formation and the Wufeng Formation.

Hydrocarbon generation of the Wufeng-Longmaxi shales started in the late Permian and the shale interval reached its maximum burial depth (>4000 m [>13,123 ft]) and temperature (>130°C [>266°F]) during the Early Jurassic–Late Cretaceous (Zeng et al., 2011; Cao et al., 2015; Guo et al., 2016). Large-scale mineral transformation in the Wufeng-Longmaxi shales likely extensively occurred

during the Jurassic, considering the burial depth, geothermal gradient, and ground temperature.

In the late stages of the Yanshan uplift and the early stages of the Himalayan uplift (Late Cretaceous–Paleogene), different regions in the Upper Yangtze block experienced different types of tectonic movements (Guo and Zeng, 2015; Zou et al., 2015). The region located to the west of the Qiyueshan thrust fault experienced compressional uplift and fold superposition, whereas the region to the east of the Qiyueshan thrust fault was affected by the Pacific tectonic system and entered its extension stage (Shen et al., 2007). In the late stages of the Himalayan uplift (Neogene–Quaternary), the entire Upper Yangtze region was in a compressional uplift stage due to the collision between the Indian plate and the China continent (Rowley, 1996). For example, according to Yan et al. (2003), currently the average shortening of the Silurian strata located to the west of the Qiyueshan thrust fault is 21.0%, whereas the average shortening of the Cambrian strata located to the east of the Qiyueshan thrust fault is 18.1%. The average shortening of the Paleozoic strata west of the Qiyueshan thrust fault is larger than that east of the Qiyueshan thrust fault. This indicates that the intensity of tectonic compaction deformation to the east of the Qiyueshan thrust fault is weaker than that to the west of the Qiyueshan thrust fault (Yan et al., 2003; Jiang et al., 2015). The SH-1 well was drilled at the northeastern wing of the Changning anticline to the south of the basin boundary, whereas the SQ-1 well is located on the saddle of an anticline close to the northeastern margin of the Jinfoshan syncline. The strata at the SH-1 and SQ-1 wells dip 33° and 4°, respectively. Except for the overlying soil, the thicknesses of the shale core from the SH-1 and SQ-1 wells are approximately 130 m (~426 ft) and 78 m (~256 ft), respectively. In addition, the JY 4 and SQ-1 wells are approximately 10 km (~6.2 mi) from the Qiyueshan thrust fault, whereas the SH-1 well is >150 km (>93 mi; Figure 1B; Table 1) farther to the west. No gas show was recorded during the drilling of either well.

SAMPLES AND METHODS

The studied samples were black shale cored from the Wufeng Formation (Ordovician) and the lower part of the Longmaxi Formation (Rhuddanian, Silurian) in the SH-1 and SQ-1 wells (Figure 1). Limestone, calcareous mudstone, and *Demirastrites triangulates* were used to identify the boundaries (Wang et al., 2015; Zheng et al., 2018) of the Wufeng Formation and the base of the Longmaxi Formation. The Wufeng Formation and Rhuddanian member of the Longmaxi Formation are the primary gas-bearing shale intervals (Zou et al., 2016a; Jia et al., 2017). In the SH-1 well, detachment layers and fractures were found to be filled with carbonate cement (Figure 2). Multiple 2-cm-thick sections were cut and collected at approximately 1.0- or 0.5-m (~1.6- or 3.3-ft) intervals throughout the shale cores, with visible fracture-sealing carbonates removed.

All of the collected core samples were divided into two aliquots, with one pulverized to 60 to 120 mesh grain sizes for low-pressure N_2 and CO_2 gas adsorption analyses, and the other powdered to less than 200 mesh grain sizes for *TOC* content and mineral composition analyses. All of the prepared samples were dried in an oven for 10 hr at 80°C (176°F) before geochemical and petrophysical analyses.

Table 1. Geological Information of Shuanghe-1, Sanquan-1, and Jiaoye 4 Wells

	SH-1	SQ-1	JY 4
Average shortening of strata	<18.1%	~18.1%	~21%
Distance from the Qiyueshan fault	>150 km (>93 mi)	~10 km (~6 mi)	~10 km (~6 mi)
Depth	157 m (515 ft)	91 m (299 ft)	2596 m (8517 ft)
Strata dip	33°	4°	<10°
Location	Exterior of Sichuan Basin	Exterior of Sichuan Basin	Interior of Sichuan Basin
Structural position	Northeastern wing of the Changning anticline	Northeastern margin of the Jinfoshan syncline	Jiaoshiba anticline

Abbreviations: JY = Jiaoye; SH = Shuanghe; SQ = Sanquan.

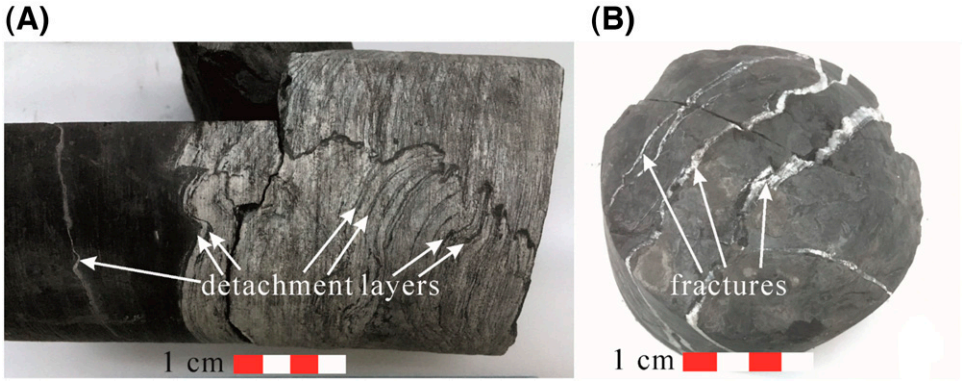

Figure 2. Photographs of selected cores showing the detachment layers and fractures filled with carbonate cement in the Wufeng Formation in the Shuanghe-1 well: (A) detachment layers at the depth of 130.7 m (428.8 ft); (B) fractures at the depth of 131.0 m (429.8 ft).

Low-pressure N_2 and CO_2 gas adsorption analyses were performed on an accelerated surface area and porosimetry system (ASAP-2460, Micromeritics Instruments), as described by Zheng et al. (2018). The specific surface area and pore volume were calculated based on the nonlocal density functional theory (NLDFT) method (Wei et al., 2016).

A total of 217 and 101 shale samples from the SH-1 and SQ-1 wells, respectively, were analyzed for their *TOC* contents using a Leco CS-320 carbon and sulfur analyzer. The <200 mesh powdered shale samples (60–100 mg) were first treated with 5% hydrochloric acid at 80°C (176°F) to remove the carbonates and then washed at least six times with deionized water to remove residual hydrochloric acid before instrumental analysis.

An x-ray diffractometer (Olympus Innova-X BTX-II) was used for mineral composition analyses. The diffractometer was equipped with a Co x-ray tube operated at 31 kV and 0.4 mA. The exposure time was 70 min and the exposure rate was 3 times/min. Stepwise scanning measurements were performed in the range of 3°–55° (2θ), using a 0.02° (2θ) scanning step. The relative mineral percentages were estimated semiquantitatively using the area under the curve for the major peaks of each mineral.

A total of 27 shale samples, 12 from the SH-1 well and 15 from the SQ-1 well, were collected from the cores for measurement of their porosity on a Micrometritics Autopore 9510 Porosimeter using the Hg injection capillary pressure (MICP) technique that has been widely used in previous studies (Ross and Bustin, 2009; Chalmers et al., 2012; Cao et al., 2015). A total of 3 to 5 g of core samples was crushed to 1–20 mesh and then dried in an oven for at least 24 hr at 110°C (230°F) under vacuum conditions. The MICP method covered the pore size ranging from 3 nm to 120 μm, and the porosities were calculated from the Hg intrusion data (Ross and Bustin, 2009). The procedure details used in this study can be found in Cao et al. (2015).

Selected shale chips were also sampled from the cores for FE-SEM imaging of the nanopores after being treated by Ar ion-beam milling (IM4000, Hitachi High-Tech). Secondary electron images for documenting topographic variation and backscattered electron images to delineate the compositional variation were acquired on Hitachi SU8010. Additional observations were made using energy-dispersive spectroscopy for mineral identification and characterization (Chalmers et al., 2012; Zhao et al., 2017a).

In addition, bulk-rock samples were selected and cut along the direction of the vertical bedding and prepared as polished blocks for petrographic observation. Due to the lack of vitrinite in the Ordovician–Silurian marine shales, pyrobitumen reflectance was measured on the blocks under reflected light with a 3Y microphotometric system for estimating their thermal maturity. When the rock is highly mature to overmature, the relationship between the pyrobitumen reflectance (R_b) and equivalent vitrinite reflectance (R_{equ}) can be expressed by the equation $R_{equ} = (R_b + 0.2443)/1.0495$ (Schoenherr et al., 2007).

RESULTS

Mineralogy

The x-ray diffraction (XRD) results indicate that the mineral composition of the Wufeng-Longmaxi shales in the SH-1 well includes quartz, feldspar, calcite, dolomite, pyrite, and clays (illite and chlorite). For the 217 samples from the SH-1 well, their clay contents are in the range of 21.0% to 52.7% (average 41.0%). Brittle minerals (quartz, feldspar, carbonates, and pyrite) are dominated by quartz (19.3%–64.8%, average 29.8%). Feldspar contents are in the range of 8.7% to 23.2%, with an average of 15.8%, and carbonate contents are in the range of 4.1% to 25.9%, with an average of 10.2%. Carbonate within the organic-rich shale intervals is dominated by calcite (1.6%–20.7%, average 7.6%) for the SH-1 well. For the 101 samples from the SQ-1 well, the clay contents are in the range of 28.8% to 54.3% (average 44.3%). Their brittle minerals are also dominated by quartz (19.6%–53.3%, average 29.0%), with feldspar contents being in the range of 10.6% to 21.5% (average of 16.4%) and carbonate contents ranging from 4.4% to 14.0%, with an average of 6.8% (Zheng et al., 2018). The calcite content within the organic-rich shale interval is in the range of 2.6% to 7.9%, with an average of 4.0% for the SQ-1 well. In JY 1, which is close to JY 4 (Figure 1), the average calcite content is 3.8% (Guo and Zhang, 2014; Guo et al., 2014), similar to the SQ-1 well. This indicates that the calcite content in the Wufeng-Longmaxi shales from the Changning area is almost twice that of the Fuling area.

Ternary diagrams in Figure 3 show the XRD mineral compositions of the Wufeng-Longmaxi shales for the SH-1 well (Figure 3A) and SQ-1 well (Figure 3B), respectively. The carbonate contents in the SH-1 well are significantly higher than those in the SQ-1 well, especially for the organic-rich shale intervals in the Wufeng and Longmaxi Formations (Figure 4). Meanwhile, in the SH-1 well, high carbonate contents in the Wufeng Formation and the base of the Longmaxi Formation are mainly contributed by calcite.

Organic Geochemistry

The *TOC* values of the core shale samples from the SH-1 well are in the range of 0.71 to 7.85 wt. %. The high-quality shale interval with *TOC* greater than 2.0 wt. % is approximately 34.5 m (~113.2 ft) thick, with an average *TOC* value of 3.9 wt. %, and it mainly occurs in the Wufeng Formation and Rhuddanian member. In addition, *TOC* values of the shale samples from above the Rhuddanian member are consistently low, ranging from 1.0 to 2.0 wt. % (Figure 4). Due to the unappealing interest in low-quality shale intervals (i.e., of <2.0 wt. % *TOC*), the following results and discussion on organic geochemical characteristics and petrophysical properties focus only on the shale samples from the Wufeng Formation and Rhuddanian member.

The OM in the Wufeng-Longmaxi shale samples is mainly composed of amorphous OM and pyrobitumen, but some graptolite periderms can be observed as well. The R_b values measured on the studied samples are between 2.53% and 2.82%, and the converted R_{equ} values vary in the range of 2.64% to 2.92%, suggesting that the Wufeng-Longmaxi shales are overmature in the SH-1 well. The thickness of the high-quality shale interval in the SQ-1 well is approximately 24 m (~79 ft), with an average *TOC* value of 3.0 wt. %, and R_{equ} values in the range of 2.14% to 2.76% (Zheng et al., 2018). The R_{equ} values of the JY 1 well, which lies close to the JY 4 well, were in the range of 2.20% to 3.06% (Guo and Zhang, 2014), indicating that the Wufeng-Longmaxi shales from SH-1, SQ-1, and JY 4 wells have experienced similar burial depths.

PETROPHYSICAL PROPERTIES

MICP Porosity

The MICP porosities of the high-quality shale intervals within the Wufeng Formation and the base of the Longmaxi Formation (Rhuddanian) are in the range of 1.79% to 5.36%, with an average of 2.78% for the SH-1 well (Table 2). The MICP porosities of the same shale interval of the SQ-1 well were in the range of 2.77% to 6.38%, with an average of 3.89% (Table 2). It is well known that OM may develop a large number of pores during hydrocarbon generation and expulsion (Jarvie et al., 2007; Chalmers et al., 2012; Milliken et al., 2013). This is reflected in our observation that MICP porosities for most of the samples in the SQ-1 well correlate with the corresponding *TOC* values, suggesting that *TOC* content

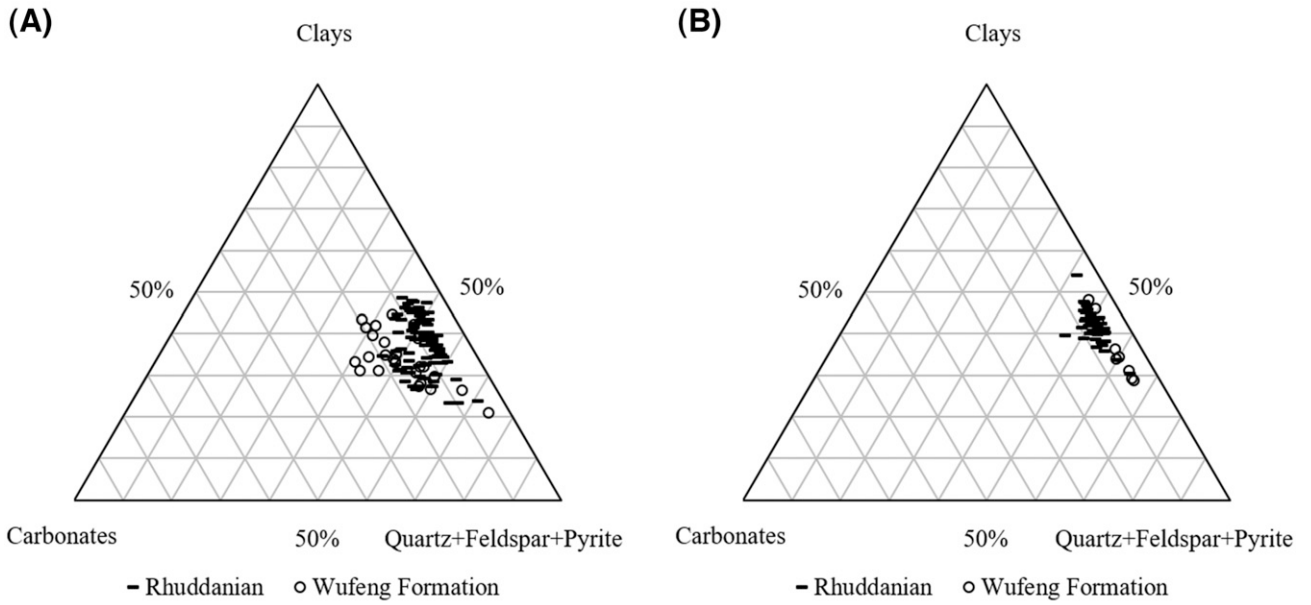

Figure 3. Ternary diagrams showing the x-ray diffraction mineralogical compositions of shale samples from the Wufeng Formation and the base of the Longmaxi Formation (Rhuddanian): (A) Shuanghe-1 well; (B) Sanquan-1 well.

is a key factor in controlling the shale reservoir quality (Figure 4). This is consistent with previous studies on the Barnett Shale (United States), the Horn River Formation (Canada), the Longmaxi Formation (China), the Marcellus Shale (United States), and the Woodford Shale (United States) using both the Hg porosimetry and low-pressure gas adsorption techniques (Chalmers et al., 2012; Milliken et al., 2013; Cao et al., 2015; Zhao et al., 2017a).

In this study, two types of porosity measured by MICP were calculated separately based on their pore size ranges: mesopores (3–50 nm) and macropores (50 nm–120 μm). Figure 4 shows that mesopore volume is dominant in MICP porosity, especially for the organic-rich shales with a carbonate content of <10%. Except for the samples with a depth of >107 m (~351 ft) that have high carbonate contents, the MICP porosities of the shale samples from the SH-1 well show a positive relationship with the corresponding *TOC* contents. Interestingly, shale samples from the high carbonate section show much lower MICP porosity. For example, a low carbonate sample SH-125a (carbonate = 7.1%, *TOC* = 4.8 wt. %) has the highest porosity, 5.36%, whereas a higher carbonate sample, SH-143a (carbonate = 11.4%, *TOC* = 4.5 wt. %), has a much lower porosity, 2.40%, despite their similar *TOC* values (Figure 4; Table 2). This indicates that shales with higher carbonate content have poorer pore connectivity because the amount of Hg injected is related to pore throat size as well (Tang et al., 2015).

Pore Volume and Specific Surface Area

The NLDFT method based on CO_2 and N_2 composited adsorption isotherms is a more suitable method for exploring the wide range of pore sizes (0.33–100 nm) of organic-rich shales (Rouquerol and Rouquerol, 2014; Wei et al., 2016). In this study, the NLDFT method was used to investigate the nanopore structure characteristics of the Wufeng-Longmaxi shales in both wells, and the results of calculated pore volume and specific surface area are presented in Table 3. The total pore volume (V_{total}) of shale from the Wufeng Formation and the Rhuddanian member of the Longmaxi Formation of the SH-1 well is in the range of 20.6 to 38.7 × 10^{-3} cm^3/g (average 29.5 × 10^{-3} cm^3/g), and 19.5 to 42.1 × 10^{-3} cm^3/g (average 30.3 × 10^{-3} cm^3/g), respectively. Their total specific surface area (S_{total}) is in the range of 18.4 to 37.2 m^2/g (average 25.8 m^2/g) and 15.2 to 43.2 m^2/g (average 26.8 m^2/g), respectively.

Figure 5 shows that pore volume (*V*) is positively correlated with *TOC* for the Wufeng-Longmaxi

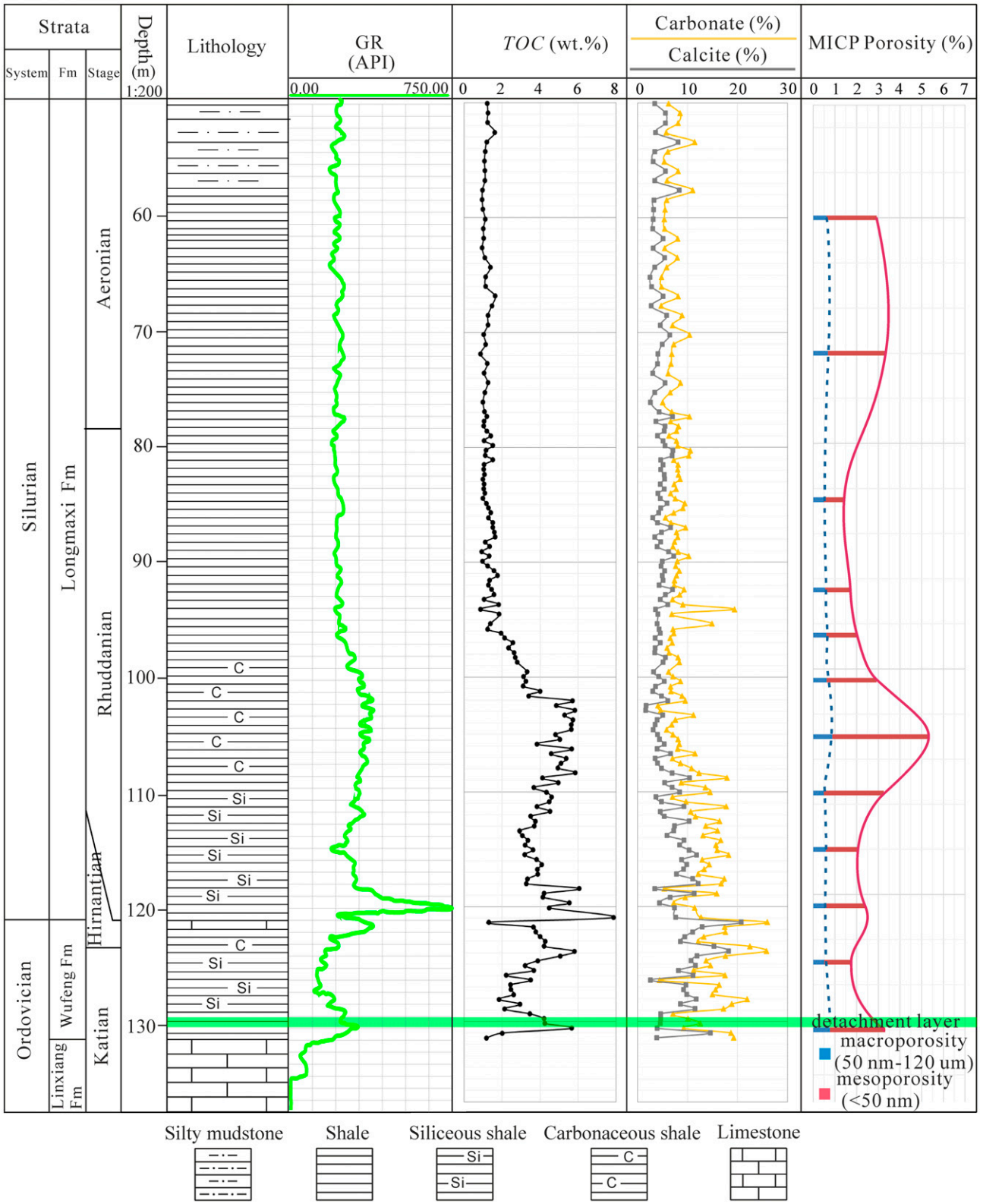

Figure 4. Depth profiles of descriptive lithology, gamma-ray (GR) logging, total organic carbon (*TOC*) contents, calcite contents, carbonate contents, and mercury injection capillary pressure (MICP) porosities of the Wufeng-Longmaxi shales for the (A) Shuanghe-1 and (B) Sanquan-1 wells. Siliceous shale: shale with a quartz content greater than 40% and *TOC* content greater than 2.0 wt. % (Liang et al., 2017); carbonaceous shale: shale with a *TOC* content greater than 3.0 wt. % (Liang et al., 2016). Fm = Formation.

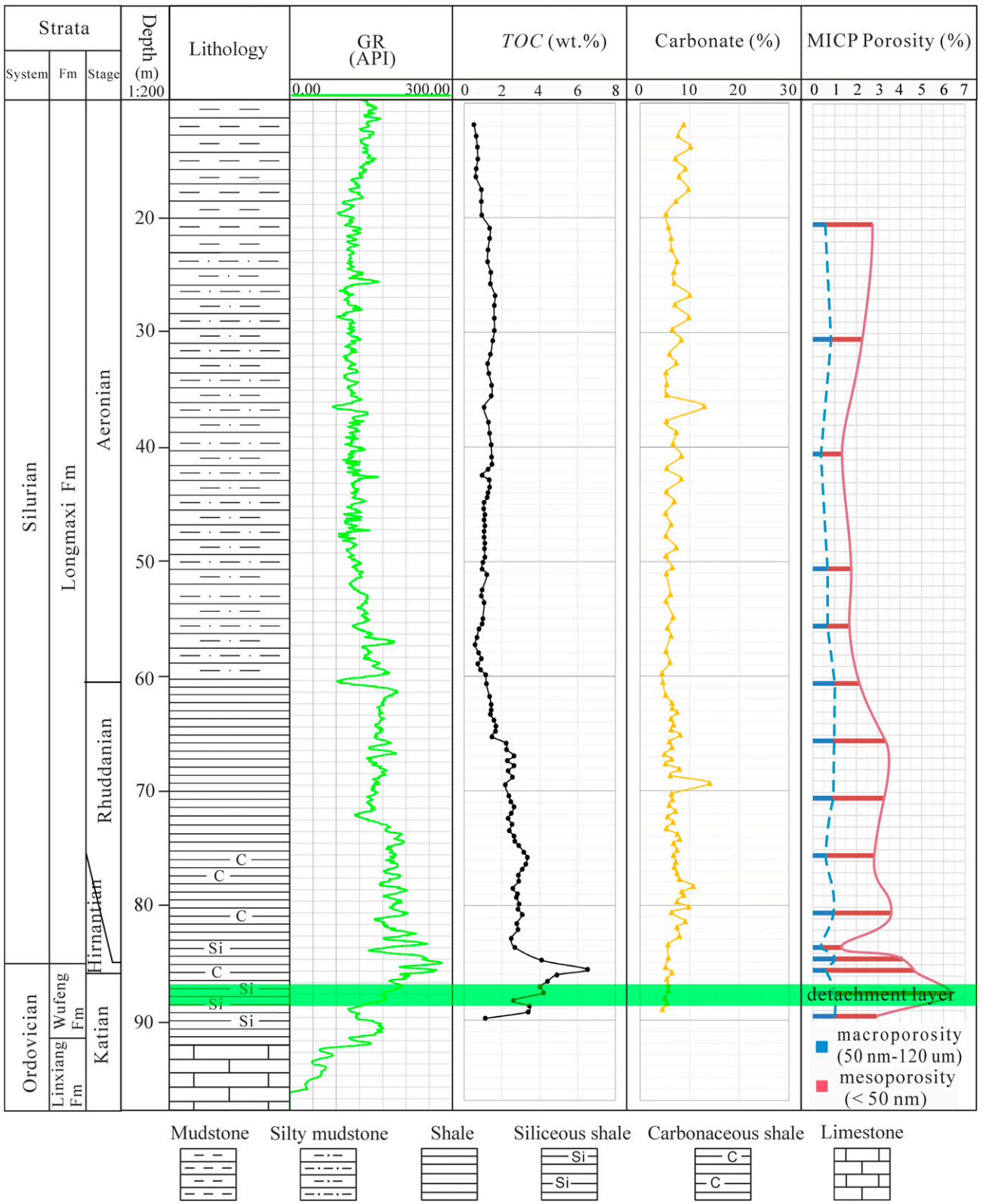

Figure 4. Continued.

Table 2. Total Organic Carbon, Carbonate Content, Mercury Injection Capillary Pressure Porosities, and Equivalent Vitrinite Reflectance of the Wufeng Formation and the Base of the Longmaxi Formation (Rhuddanian) in the Shuanghe-1 and Sanquan-1 Wells

Samples	Depth, m (ft)	*TOC*, wt. %	Carbonate, %	Porosity, %	Mesoporosity, %	Macroporosity, %	R_{equ}, %
SH-1 well							
SH-85	71.9 (235.9)	0.87	6.8	3.34	2.65	0.69	2.76
SH-100a	84.0 (275.6)	1.10	6.6	1.43	0.94	0.49	–
SH-110a	92.4 (303.1)	1.44	9.3	1.71	1.15	0.56	–
SH-115a	96.6 (316.9)	2.13	6.5	2.04	1.43	0.61	–
SH-120a	100.8 (330.7)	3.11	6.6	2.91	2.30	0.62	2.92
SH-125a	105.0 (344.5)	4.80	7.1	5.36	4.48	0.88	–
SH-131a	110.0 (360.9)	4.33	14.5	3.25	2.76	0.49	2.64
SH-138a	115.9 (380.2)	3.81	12.9	2.04	1.46	0.58	–
SH-143a	120.1 (394.0)	4.48	11.4	2.40	1.84	0.56	–
SH-147a	123.5 (405.2)	4.20	22.5	1.95	1.34	0.61	–
SH-149a	125.1 (410.4)	3.22	14.6	1.79	1.28	0.51	2.87
SH-156a	131.0 (429.8)	2.00	18.7	3.31	2.54	0.78	–
SQ-1 well							
SQ-60	60.5 (198.4)	1.18	4.6	2.17	1.16	1.01	2.14
SQ-65	65.7 (215.4)	2.23	5.9	3.37	2.41	0.96	–
SQ-70	70.8 (232.1)	2.48	6.5	3.29	2.40	0.89	–
SQ-75	75.6 (248.1)	3.34	6.7	2.77	2.15	0.62	–
SQ-80	80.6 (264.4)	3.07	6.3	3.62	2.67	0.94	2.56
SQ-84	84.6 (277.4)	4.11	5.7	4.12	3.17	0.95	2.26
SQ-85	85.4 (280.1)	6.53	5.1	4.66	4.07	0.59	2.38
SQ-87	86.4 (283.5)	3.41	5.4	6.38	5.35	1.03	2.65
SQ-89	89.1 (292.2)	3.40	4.5	2.94	1.97	0.97	–

Abbreviations: R_{equ} = equivalent vitrinite reflectance; SH = Shuanghe; SQ = Sanquan; *TOC* = total organic carbon.

shale samples from the SH-1 (with carbonate content <10%), SQ-1 (Zheng et al., 2018), and JY 4 (Wei et al., 2016) wells. More important, the positive correlation holds best for micropores (Figure 5A). Both mesopore and macropore volumes of the Wufeng-Longmaxi shales are larger in the SH-1 well (with carbonate content <10%) than in the JY 4 and SQ-1 wells. In addition, the studied shale samples fall more scattered on the *V* versus *TOC* crossplots in Figure 5 with increasing *TOC*, especially at *TOC* ≥ 3.0 wt. % and for mesopore and macropore volumes, and this is most apparent for samples from the SH-1 well (Figure 5B, C). As shown in Figure 6, the specific surface area (*S*) is also positively correlated with *TOC* for the shale samples from SH-1 (with carbonate content <10%), SQ-1, and JY 4 wells, especially for micropores (Figure 6A). Remarkably, similar positive linear relationships exist between the S_{total} values and *TOC* contents for all three wells (Figure 6D).

In the SH-1 well, however, the Wufeng Formation and the base of the Longmaxi Formation contain high contents of carbonate (10% or more; Figure 4). To elucidate the influence of carbonate cement on petrophysical properties, the Wufeng-Longmaxi shale samples from the SH-1 well were divided into two subsets: one with carbonate <10% and the other with carbonate ≥10% (Table 3). It is obvious from Figures 7 and 8 that shale samples containing fewer (<10%) carbonates populate above those with higher (>10%) carbonates on both the *V* versus *TOC* and *S* versus *TOC* crossplots.

FE-SEM of Shales

Figures 9–12 present the FE-SEM images and energy-dispersive spectroscopy results of 4 samples, SH-125a, SH-141a, SH-143a, and SH-147a, from the SH-1 well. Sample SH-125a with a carbonate of 7.1% and *TOC* of 4.8 wt. % is from the middle of the Rhuddanian member and displays the highest MICP porosity. Its detrital grains commonly show point-to-line contact (Figure 9A), and the primary

Table 3. Pore Structure Parameters in the Shuanghe-1 Well Obtained by the Nonlocal Density Functional Theory Method

				Composited N_2 and CO_2 NLDFT Model							
				Pore Volumes (10^{-3} ml/g)				Surface Areas (m^2/g)			
Sample	Depth, m (ft)	*TOC*, wt. %	Carbonate, %	V_{mic}	V_{mes}	V_{mac}	V_{total}	S_{mic}	S_{mes}	S_{mac}	S_{total}
Subset 1											
SH-60	50.9 (167.0)	1.25	8.5	5.15	15.18	1.86	22.19	14.85	3.92	0.05	18.82
SH-70	59.3 (194.5)	1.00	5.5	4.58	16.01	1.41	22.00	13.33	4.01	0.03	17.37
SH-80	67.7 (222.0)	1.46	4.7	5.52	19.48	2.16	27.16	16.33	4.58	0.05	20.96
SH-85	71.9 (235.8)	0.87	6.8	4.48	14.54	1.68	20.70	12.97	3.39	0.04	16.41
SH-95a	79.9 (262.0)	1.51	8.0	5.19	16.45	2.34	23.98	15.04	4.07	0.06	19.16
SH-100	84.0 (275.6)	1.10	6.6	4.08	14.05	2.11	20.24	12.25	2.88	0.07	15.20
SH-110	92.4 (303.1)	1.44	9.3	4.49	12.67	2.29	19.45	13.23	2.89	0.07	16.19
SH-115	96.6 (317.0)	2.13	6.5	6.08	20.69	4.15	30.92	17.46	4.58	0.13	22.17
SH-116a	97.5 (319.7)	2.34	5.9	6.77	24.14	4.54	35.45	19.75	5.48	0.11	25.33
SH-119a	100.0 (328.0)	3.12	7.1	8.00	27.10	4.69	39.79	23.14	6.27	0.12	29.52
SH-120a	100.8 (330.7)	3.11	6.6	8.33	27.53	4.76	40.62	23.95	6.29	0.15	30.39
SH-120b	101.2 (332.1)	3.99	6.7	8.77	23.28	2.90	34.96	25.45	6.19	0.07	31.71
SH-121a	101.6 (333.5)	3.39	8.9	8.77	24.90	4.06	37.73	24.76	6.16	0.13	31.05
SH-121b	102.1 (334.9)	5.70	9.5	11.69	25.10	3.19	39.99	34.66	6.79	0.08	41.53
SH-122a	102.5 (336.2)	4.85	4.1	11.13	38.61	6.04	55.78	37.27	8.06	0.19	45.52
SH-122b	102.9 (337.6)	5.83	4.6	10.91	26.93	3.42	41.26	31.65	7.01	0.08	38.74
SH-123b	103.7 (340.4)	5.73	7.5	10.00	26.98	3.26	40.24	29.38	6.87	0.08	36.33
SH-125a	105.0 (344.5)	4.80	7.1	9.66	28.90	3.57	42.13	27.81	6.81	0.08	34.70
SH-126a	105.8 (347.2)	3.84	8.3	8.09	22.87	3.91	34.87	24.46	5.52	0.10	30.07
SH-127b	107.1 (351.4)	5.37	7.0	9.90	31.88	6.50	48.28	30.23	7.00	0.16	37.39
SH-130a	109.2 (358.3)	4.95	8.7	8.52	21.20	2.97	32.69	26.24	5.22	0.07	31.53
SH-132a	110.9 (363.8)	4.48	9.7	7.63	20.84	3.52	31.99	23.50	4.77	0.09	28.36
SH-141a	118.4 (388.5)	6.06	5.3	9.02	21.10	3.19	33.31	28.67	5.05	0.08	33.80
SH-142a	119.2 (391.0)	4.15	9.5	6.61	18.22	2.61	27.44	20.62	4.23	0.06	24.91
SH-142b	119.7 (392.6)	5.54	7.2	9.26	24.10	3.66	37.02	28.87	5.46	0.10	34.42
Subset 2											
SH-123a	103.3 (339.0)	5.29	11.2	10.28	25.95	3.62	39.85	30.54	6.57	0.09	37.20
SH-127a	106.7 (350.0)	4.58	11.5	9.82	25.77	2.92	38.51	28.05	6.10	0.07	34.22
SH-128b	107.9 (354.1)	4.93	10.8	10.66	28.36	4.02	43.04	32.34	6.81	0.10	39.25
SH-131a	110.0 (361.0)	4.33	14.5	7.61	21.36	3.43	32.40	23.15	5.11	0.08	28.34
SH-133a	111.7 (366.5)	4.51	10.6	7.61	21.10	3.81	32.52	23.64	4.74	0.10	28.48
SH-134a	112.5 (369.3)	3.74	16.4	6.65	17.58	3.03	27.26	20.76	4.12	0.07	24.95
SH-135a	113.4 (372.0)	2.91	16.0	5.86	16.16	2.99	25.00	17.91	3.72	0.09	21.72
SH-136a	114.2 (374.8)	3.35	16.6	5.67	15.88	2.55	24.10	17.53	3.62	0.06	21.21
SH-138a	115.9 (380.3)	3.81	12.9	5.92	14.35	2.32	22.59	18.46	3.38	0.06	21.90
SH-139a	116.7 (383.0)	3.85	13.3	6.40	16.72	2.75	25.87	19.65	3.99	0.07	23.71
SH-139b	117.2 (384.4)	3.87	12.1	6.95	19.36	3.36	29.67	22.10	4.43	0.08	26.61
SH-140a	117.6 (385.8)	3.34	17.3	5.72	15.18	2.48	23.38	17.39	3.63	0.06	21.08
SH-143a	120.1 (394.0)	4.48	11.4	6.95	17.89	1.46	26.30	21.36	4.27	0.04	25.66
SH-146a	122.6 (402.3)	3.99	13.2	7.55	22.12	4.29	33.96	23.43	4.80	0.10	28.34
SH-147a	123.5 (405.0)	4.21	22.5	7.40	20.71	3.46	31.58	23.37	4.48	0.09	27.95
SH-148a	124.3 (407.8)	5.05	17.6	7.78	17.04	2.76	27.58	24.62	3.96	0.07	28.65
SH-149a	125.1 (410.5)	3.22	14.6	5.85	17.90	3.31	27.06	17.80	3.93	0.08	21.81
SH-153a	128.5 (421.5)	2.94	18.8	6.22	19.52	2.32	28.06	17.89	4.54	0.06	22.49
SH-156a	131.0 (429.8)	2.00	18.7	5.02	20.38	2.92	28.32	14.18	4.17	0.07	18.43

Abbreviations: NLDFT = nonlocal density functional theory; SH = Shuanghe; S_{mac} = the macropore specific surface area; S_{mes} = mesopore specific surface area; S_{mic} = micropore specific surface area; $S_{total} = S_{mic} + S_{mes} + S_{mac}$; V_{mac} = macropore volume; V_{mes} = mesopore volume; V_{mic} = micropore volume; $V_{total} = V_{mic} + V_{mes} + V_{mac}$.

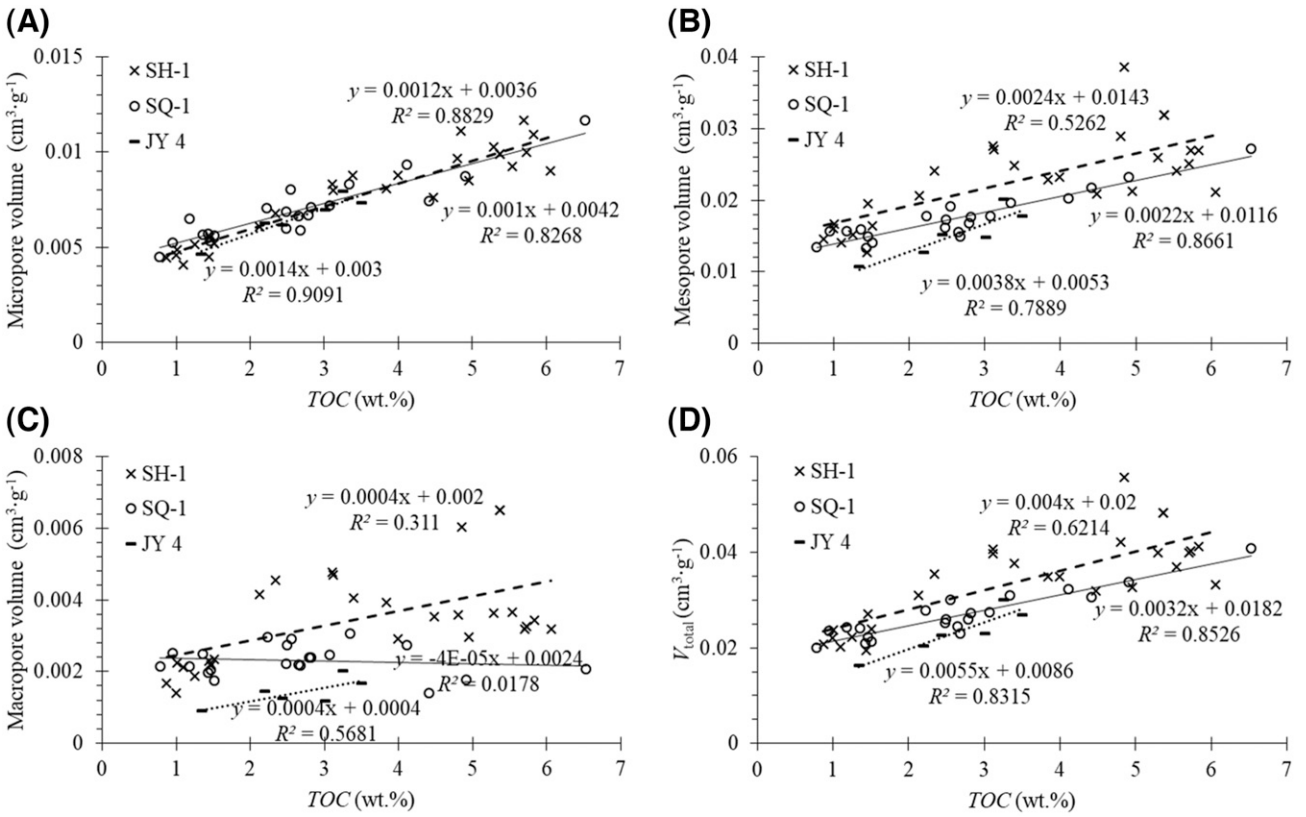

Figure 5. Relationship between nanopore volumes and total organic carbon (*TOC*) contents for Wufeng-Longmaxi shales from the Shuanghe-1 (SH-1), Sanquan-1 (SQ-1) (Zheng et al., 2018), and Jiaoye 4 (JY 4) (Wei et al., 2016) wells. (A) Micropore volume (V_{mic}) versus *TOC*; (B) mesopore volume (V_{mes}) versus *TOC*; (C) macropore volume (V_{mac}) versus *TOC*; and (D) total pore volume ($V_{total} = V_{mic} + V_{mes} + V_{mac}$) versus *TOC*. R^2 = coefficient of determination.

interparticle pores in SH-125a are almost fully cemented by authigenic quartz under FE-SEM (Figure 9D). Its OM grains are darker than minerals under FE-SEM (Figure 9) and can be classified into depositional OM (kerogen) and migrated OM (pyrobitumen) (Loucks and Reed, 2014). Kerogen macerals are commonly in direct contact with the detrital mineral grains (Bernard et al., 2012; Loucks and Reed, 2014). In addition, graptolite periderms, which were commonly preserved in the voids of fossil bodies (Figure 9C) (Ma et al., 2016), appear to be one of the most important source materials for kerogen in the Wufeng-Longmaxi shales. Figure 9D shows that only a few organic pores with diameters >50 nm developed in the graptolite periderms. However, pyrobitumen, commonly occurring in the aggregates of authigenic microcrystalline quartz (Loucks and Reed, 2014; Zhao et al., 2017a), are usually porous OM grains that contain abundant mesopores and macropores (Figure 9A, B, D). One large piece of OM in Figure 9B has 35% visible porosity (by the point-count method), whereas the visible porosity of the whole shale sample SH-125a is only 4.8% on the basis of 1000 point counts. Furthermore, OM pores with large pore size are usually observed among the rigid detrital quartz grains (Figure 9A). The largest macropores can have a measured length of up to 1400 nm, and they can connect many pores, obviously improving the connectivity of the pore networks (Figure 9B). It is also noteworthy that some of the OM pores are elongated, showing preferential orientation (Figure 9A, B).

Milliken et al. (2013) reported that the Devonian Marcellus Shale samples with *TOC* > 5.5 wt. % show little or no increase in the porosity with a further increasing *TOC*. This phenomenon has also been observed in the present study. For example, the visible porosity of the shale sample SH-141a with a carbonate content of 5.3% and a *TOC* content of 6.1% is 2.3% on the basis of 1000 point counts,

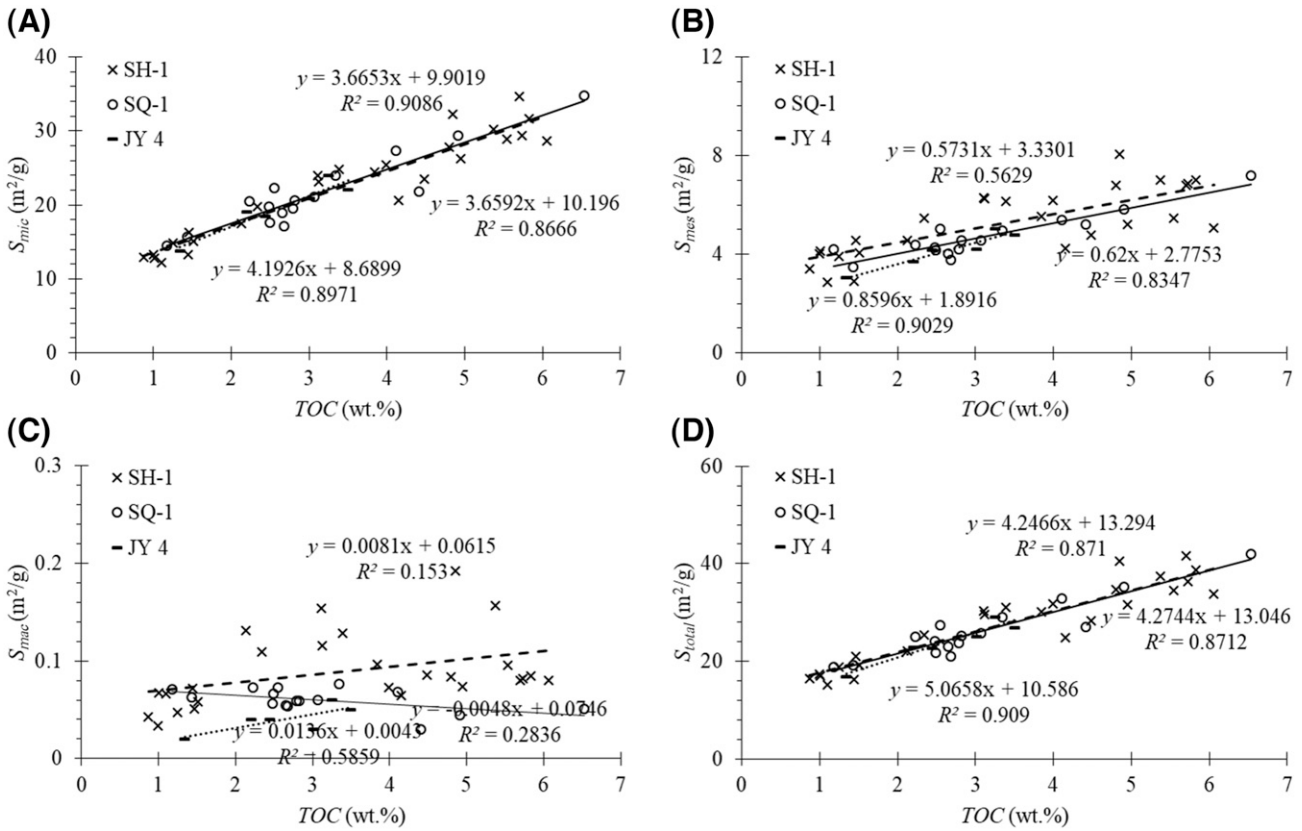

Figure 6. Relationship between specific surface areas of nanopores and total organic carbon (*TOC*) contents for shales from the Shuanghe-1 (SH-1), Sanquan-1 (SQ-1) (Zheng et al., 2018), and Jiaoye 4 (JY 4) (Wei et al., 2016) wells. (A) Micropore specific surface area (S_{mic}) versus *TOC*; (B) mesopore specific surface area (S_{mes}) versus *TOC*; (C) macropore specific surface area (S_{mac}) versus *TOC*; and (D) total pore specific surface area ($S_{total} = S_{mic} + S_{mes} + S_{mac}$) versus *TOC*. R^2 = coefficient of determination.

much lower than that of sample SH-125a, with a carbonate content of 7.1% and a lower 4.8% *T*OC. The SEM imaging shows that the spaces between detrital grains in SH-141a were mostly either filled by OM or cemented by authigenic quartz (Figure 10A–C). It is also clear that the OM patches contain many more mesopores than macropores (Figure 10D). In addition, the feldspar particles show corroded margins, indicating that they were partly dissolved (Figure 10B, C). This could have been caused by the organic acids and CO_2 formed from OM during its hydrocarbon generation because these compounds can destroy and dissolve unstable mineral grains such as feldspar and carbonate (MacGowan and Surdam, 1990; Morad et al., 2010; Schieber, 2010; Ma et al., 2017). A total mineral dissolution would result in a pore of the same size and shape as the dissolved particle (Figure 10E), and this type of pore was called moldic pore (Choquette and Pray, 1970; Lucia, 1995; Loucks et al., 2012). The moldic pore shown in Figure 10E is surrounded by clay and filled with migrated OM or bitumen in which only mesopores could be observed (Figure 10F). Based on the shape of the moldic pore, the completely dissolved mineral was likely calcite.

Figures 11 and 12 show the FE-SEM images of samples SH-143a (carbonate = 11.4%, *T*OC = 4.5 wt. %) and SH-147a (carbonate = 22.5%, *T*OC = 4.2 wt. %) to illustrate the influence of carbonate cement on organic pores. Large calcite grains with corroded edges have been observed (Figure 11A). Interparticle pores are dominantly filled with authigenic quartz and migrated OM. The migrated OM or bitumen patches, occurring among the aggregates of authigenic microcrystalline quartz or near the detrital quartz, are rich in various types of mesopores and macropores (Figure 11C, D). The organic pores in the migrated OM are mostly less than 100 nm in dimension and of round shapes (Figure 11D). Only a few pores are visible in graptolite periderms

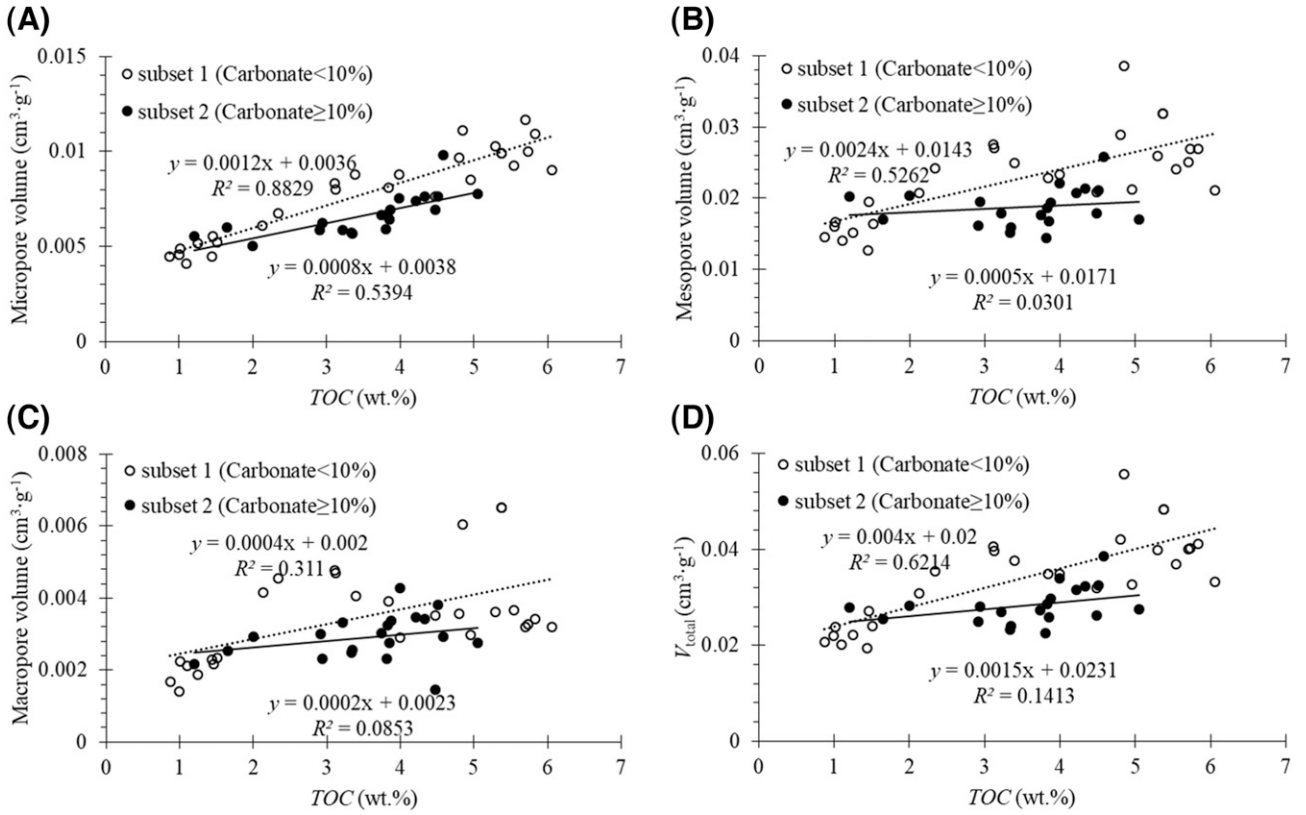

Figure 7. Relationship between nanopore volume and total organic carbon (*TOC*) contents for shale samples from the Shuanghe-1well grouped according to their carbonate contents. (A) Micropore volume (V_{mic}) versus *TOC*; (B) mesopore volume (V_{mes}) versus *TOC*, showing a large deviation of the mesopore volume off the regression line; (C) macropore volume (V_{mac}) versus *TOC*; and (D) total pore volume ($V_{total} = V_{mic} + V_{mes} + V_{mac}$) versus *TOC*. Subset 2 samples with carbonate contents $\geq$10% populate beneath the regression line of subset 1 samples of lower carbonate contents (<10%), indicating that higher carbonate contents lead to lower nanopore volumes. R^2 = coefficient of determination.

(Figure 11E, F). The large piece of OM grains in Figure 11C, likely pyrobitumen, has 12% visible porosity by SEM point counts, whereas the OM grains in Figure 11F, a piece of graptolite periderm, has only 0.1% visible porosity. In addition, organic pores are rare in the part of the OM near calcite (Figure 11B).

Figure 12 shows that with increasing carbonate content, the interparticle pores seem to be increasingly filled with calcite cement rather than authigenic quartz. In a two-dimensional view, the carbonate grains dominantly show line-to-mosaic contact (Figure 12A–C, E). The dissolved carbonates seemed to have recrystallized as carbonate cement within the interparticle pores, thus mostly taking blocky shapes (Figure 12A, B). As a result, shales containing a higher content of calcite became more compacted relative to shales rich in porous OM grains and authigenic quartz. Such a trend is clearly shown by FE-SEM images of the shale samples SH-125a (Figure 9), SH-143a (Figure 11), and SH-147a (Figure 12), which have similar *TOC* values (4.8%, 4.5%, and 4.2%, respectively) but varying carbonate contents (7.1%, 11.4%, and 22.5%, respectively). The amount of the OM grains and authigenic quartz in SH-147a were significantly reduced, and some of its OM grains were even isolated from the shale pore networks by carbonate cement (Figure 12A, B).

Among the four SEM-imaged shale samples, secondary enlargement of calcite was also commonly observed in the most carbonate-rich sample, SH-147a (Figure 12C). In addition, a devolatilization microcrack in the OM patch was found to be partially filled with calcite cement on sample SH-147a (Figure 12D), suggesting that intensive carbonate cementation may reduce the connectivity of the pore networks of the shales. Despite their similar thermal maturation history, organic pores in the migrated OM or pyrobitumen in SH-147a (e.g., Figure 12F) is

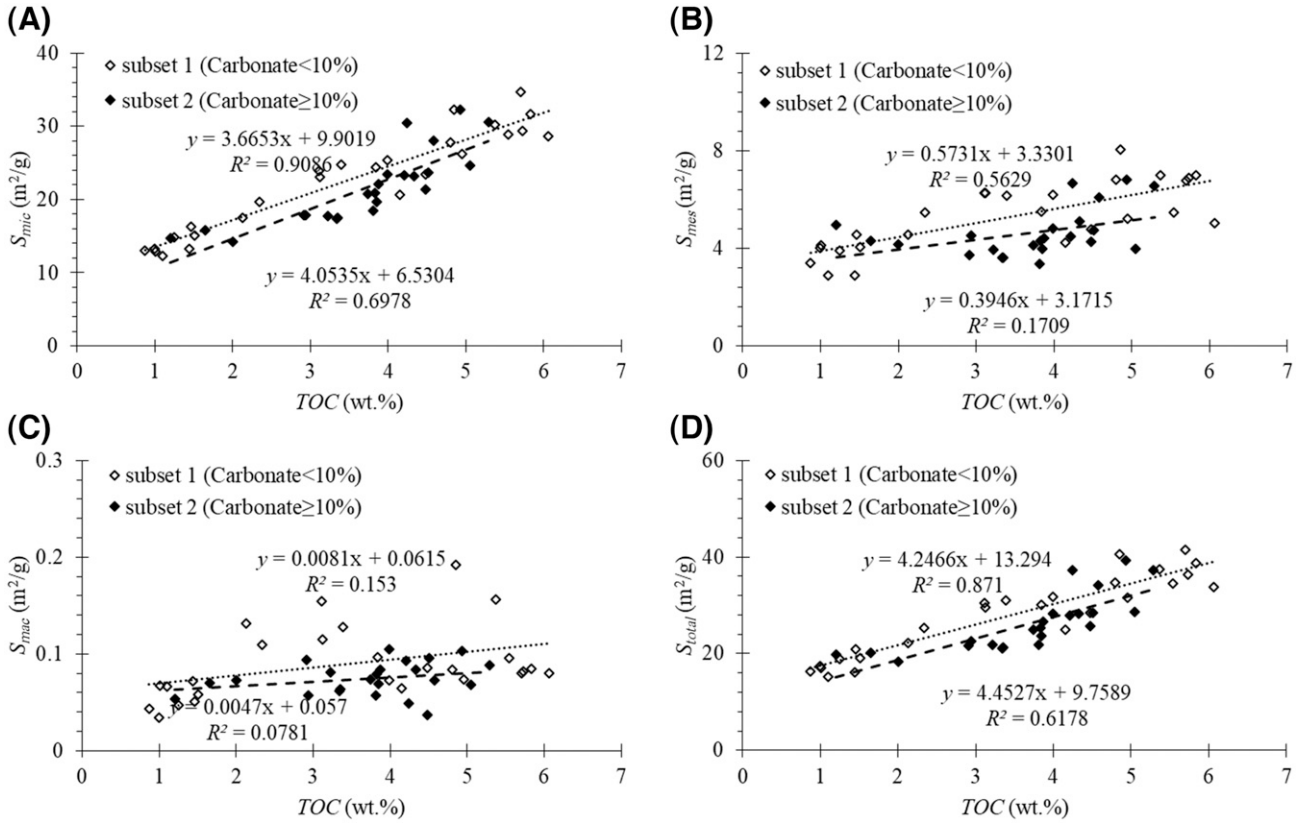

Figure 8. Relationship between specific surface area of nanopores and total organic carbon (*TOC*) contents for shale samples from the Shuanghe-1 well grouped according to their carbonate contents. (A) Micropore specific surface area (S_{mic}) versus *TOC*; (B) mesopore specific surface area (S_{mes}) versus *TOC*; (C) Macropore specific surface area (S_{mac}) versus *TOC*; and (D) total pore specific surface area ($S_{total} = S_{mic} + S_{mes} + S_{mac}$) versus *TOC*. Subset 2 samples with carbonate contents ≥10% populate beneath the regression line of subset 1 samples of lower carbonate contents (<10%), indicating that higher carbonate contents lead to the lower nanopore specific surface area. R^2 = coefficient of determination.

not as large as that in SH-125a (e.g., Figure 9B). Consequently, the MICP porosity is only 1.95% for SH-147a, 2.40% for SH-143a, and 5.36% for SH-125a in the order of decreasing content of carbonate. Therefore, shale with intensive carbonate cementation has significantly lower porosity than shale with lower carbonate contents.

DISCUSSION

Factors Controlling the Wufeng-Longmaxi Shale Gas Content between Changning and Fuling Fields

The Wufeng-Longmaxi shale intervals from the southern Sichuan Basin (e.g., the SH-1 well in Changning field) and the eastern Sichuan Basin (e.g., the JY 1 and JY 4 wells in the Fuling field, the SQ-1 well near Fuling field) have many similarities in their sedimentary environments and geochemical parameters (Figure 13). For example, the high-quality (*TOC* > 2.0 wt. %) shale intervals in the SH-1 well are approximately 34.5 m (~113.2 ft) thick, with an average *TOC* value of 3.9 wt. %, whereas the total thickness of the high-quality shale intervals in JY 1 is approximately 38.0 m (~124.7 ft), with an average *TOC* of 3.5 wt. % (Guo and Zhang, 2014). The equivalent vitrinite-reflectance values of the SH-1 and JY 1 wells are in the ranges of 2.64% to 2.92% and 2.20% to 3.06% (Guo and Zhang, 2014), respectively. Furthermore, the average brittle mineral content of the high-quality shale intervals in the SH-1 well is 64.5%, only slightly higher than that of JY 1 (62.4%). Therefore, the Wufeng-Longmaxi shale intervals in the Changning and Fuling fields appear to

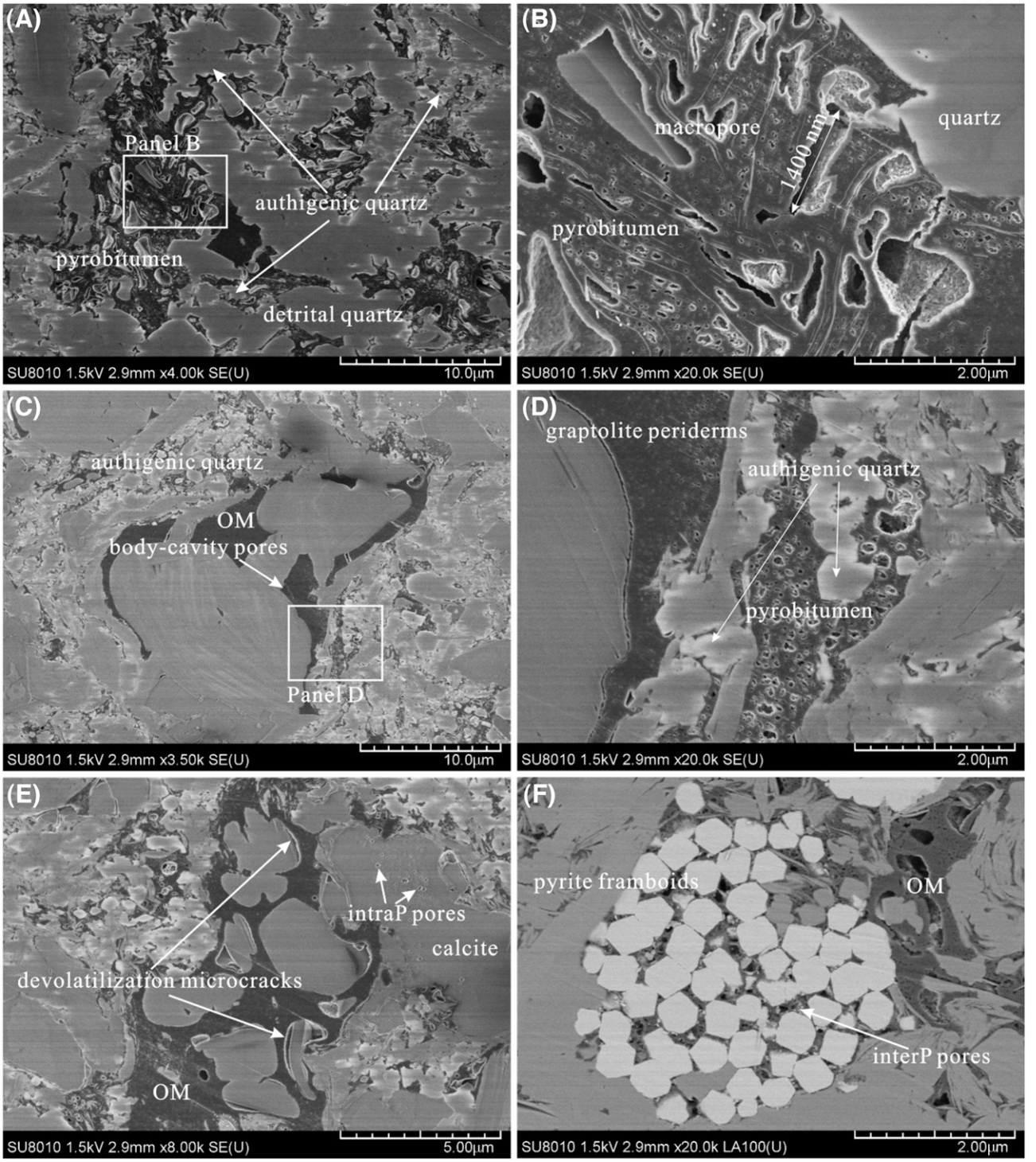

Figure 9. Field emission-scanning electron microscopy images for sample Shuanghe-125a (carbonate 7.1%, total organic carbon = 4.8 wt. %). (A) Interparticle pores among the detrital grains were mostly filled with the aggregates of authigenic microcrystalline quartz; (B) macropores in pyrobitumen with pore size up to 1400 nm in length connecting many pores; (C) voids of fossil bodies and graptolite periderms; (D) pyrobitumen rich in various types of mesopores and macropores, and graptolite periderms with mesopores of small sizes; (E) intraparticle (intraP) pores in calcite grains; and devolatilization microcracks between the organic matter (OM) grains and mineral particles; (F) interparticle (interP) pores among the pyrite framboids. See Table 2 for more sample information.

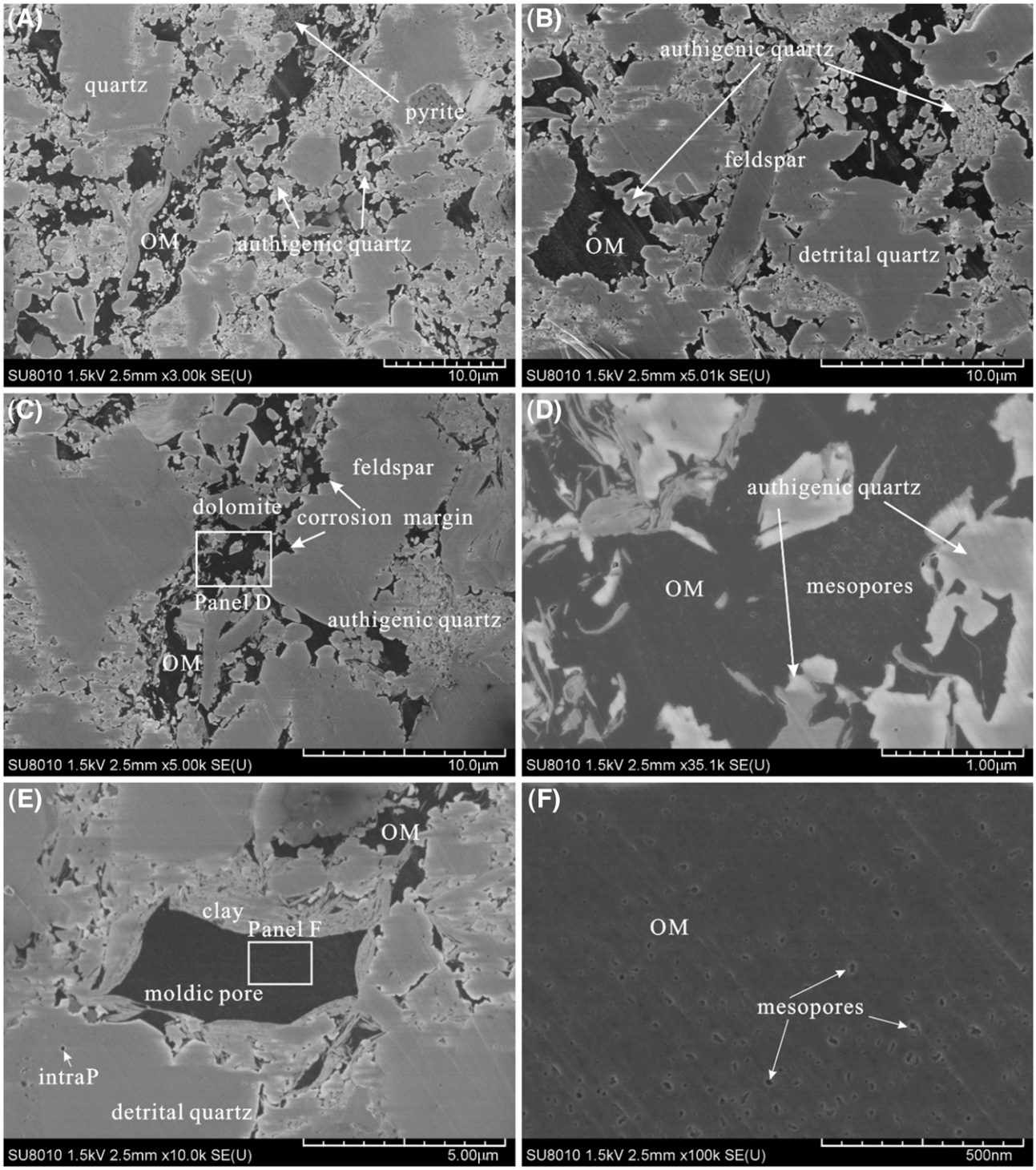

Figure 10. Field emission-scanning electron microscopy images for sample Shuanghe-141a (carbonate 5.3%, total organic carbon [*TOC*] = 6.1 wt. %). (A, B) Mineral particles almost dispersed in organic matter (OM). Primary particle pores are dominantly cemented by authigenic quartz; (C) irregular embay outline of feldspar grains; (D) OM grains containing few mesopores; (E) moldic pore likely resulting from calcite dissolution and refilled with OM; (F) mesopores in the OM grain filled in a moldic pore. intraP = intraparticle. See Table 2 for more sample information.

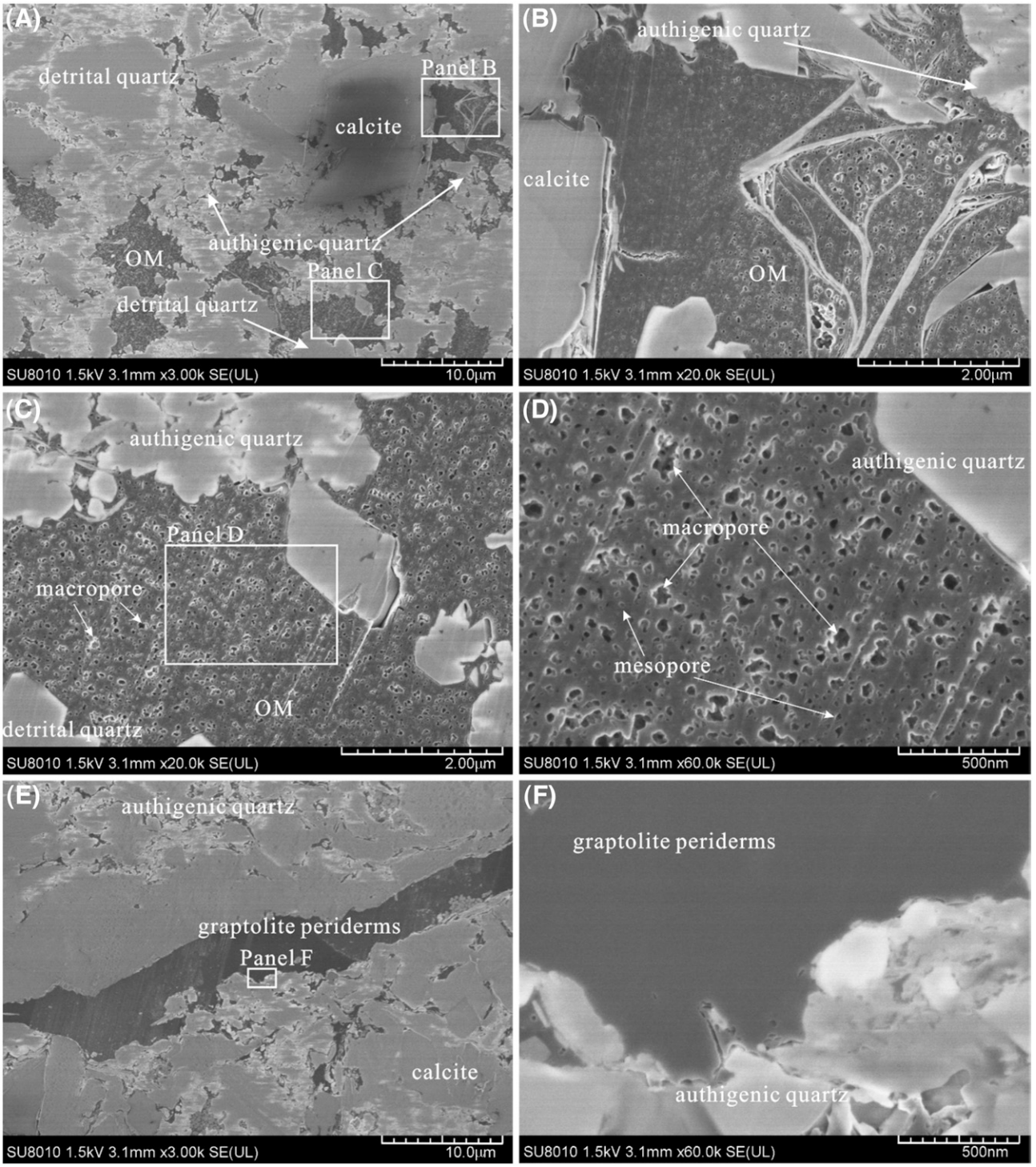

Figure 11. Field emission-scanning electron microscopy images for sample Shuanghe-143a (carbonate = 11.4%, total organic carbon = 4.5 wt. %). (A) Interparticle pores among the detrital grains filled with authigenic quartz. A large calcite grain was partially dissolved showing the dissolution edges; (B) organic matter (OM) pores being less developed near calcite than near authigenic quartz; (C, D) OM patches rich in various types of mesopores and macropores; (E, F) graptolite periderms with limited visible pores. See Table 2 for more sample information.

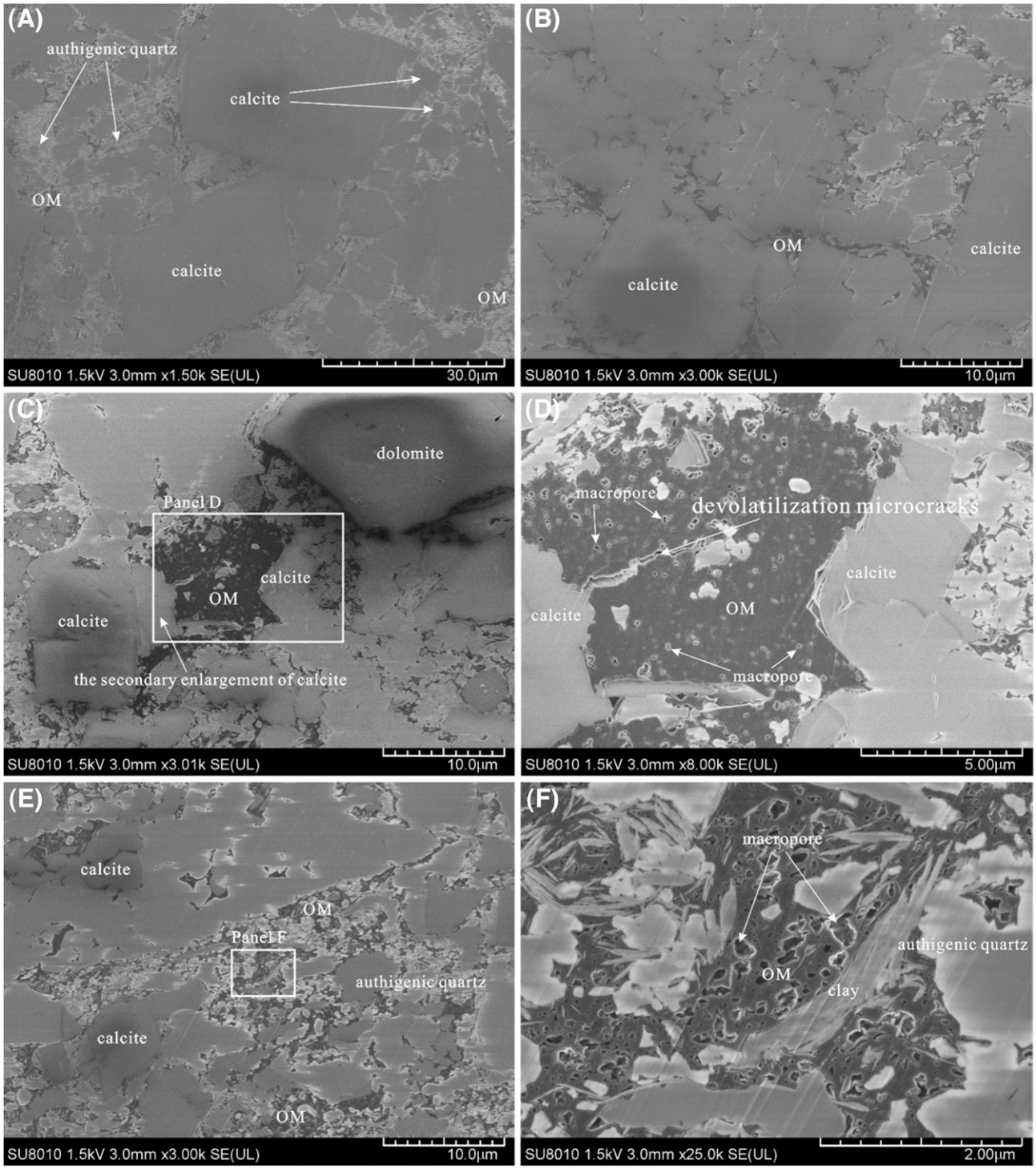

Figure 12. Field emission-scanning electron microscopy images for sample Shuanghe-147a (carbonate = 22.5%, total organic carbon = 4.2 wt. %). (A) Blocky carbonate cements. (B) Mineral particles showing the line and mosaic contact. Carbonate cements became heavily compacted, and many organic matter (OM) grains were isolated from the pore networks of shale. (C, D) OM grain containing less developed OM pores near carbonate cements. (E) Primary interparticle pores filled with authigenic quartz. (F) Pyrobitumen occurring in the aggregates of authigenic microcrystalline quartz rich in various types of mesopores and macropores. See Table 2 for more sample information.

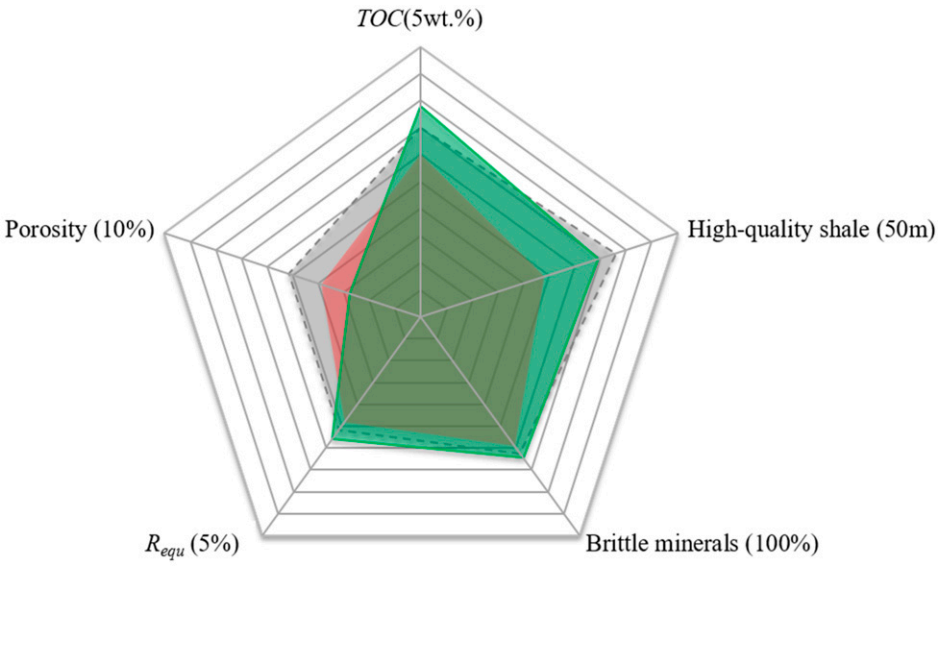

	JY 1	SQ-1	SH-1
TOC (wt.%)	3.5	3.0	3.9
High-quality shale (m)	38.0	24.0	34.5
Brittle minerals (%)	62.4	59.1	64.5
R_{equ} (%)	2.20-3.06 (2.6)	2.14-2.76 (2.4)	2.6-2.9 (2.8)
Porosity (%)	5.1	3.9	2.8

Figure 13. A star diagram comparing the shale reservoir properties of the Wufeng-Longmaxi shales from the Jiaoye 1 (JY 1), Sanquan -1 (SQ-1), and Shuanghe-1 (SH-1) wells. Brittle minerals include quartz, feldspar, carbonates, and pyrite, and high-quality shale represents shales with a total organic carbon (*TOC*) content >2.0 wt. %. R_{equ} = equivalent vitrinite reflectance.

have similar hydrocarbon generation potentials based on their thickness, TOC contents, OM type, maturity level, and brittle mineral content.

Despite their similar hydrocarbon generation potentials, the shale gas content is found to be significantly lower in the Changning shale gas field (2.4–5.5 m^3/t, 84.8–194.2 ft^3/t) than in the Fuling shale gas field (4.7–7.2 m^3/t, 166.0–254.3 ft^3/t) (Zhao et al., 2016b; Zou et al., 2016a). The current results of shale gas exploration and production in South China show that pressure coefficient can be an indicator of preservation (Guo and Zhang, 2014; Zou et al., 2016a). A higher pressure coefficient usually means better preservation (Guo and Zhang, 2014). However, preservation does not seem to be the main factor for the shale gas content of the Wufeng-Longmaxi shales in the Changning shale gas field because the pressure coefficient of the Changning shale gas field (1.25–2.10) is actually higher than that of the Fuling shale gas field (1.35–1.55); that is, the Changning gas field has better gas preservation than the Fuling gas field. This further suggests that the difference in the gas contents of the Wufeng-Longmaxi shale intervals between the Changing and Fuling gas fields has other more important causes than source rock hydrocarbon generation capacity and reservoir preservation, and the difference in the average porosities of the high-quality shale intervals between the Changning and Fuling fields are likely one such critical factor. For example, the average porosity of the SH-1 well (i.e., 2.9%; Table 2) is significantly lower than that of the JY 1 well (i.e., 5.1%; Figure 13), meaning that the Wufeng-Longmaxi shale reservoir has much lower storage capacity in the Changning field than in the Fuling field, and hence, lead to the sharp contrast in

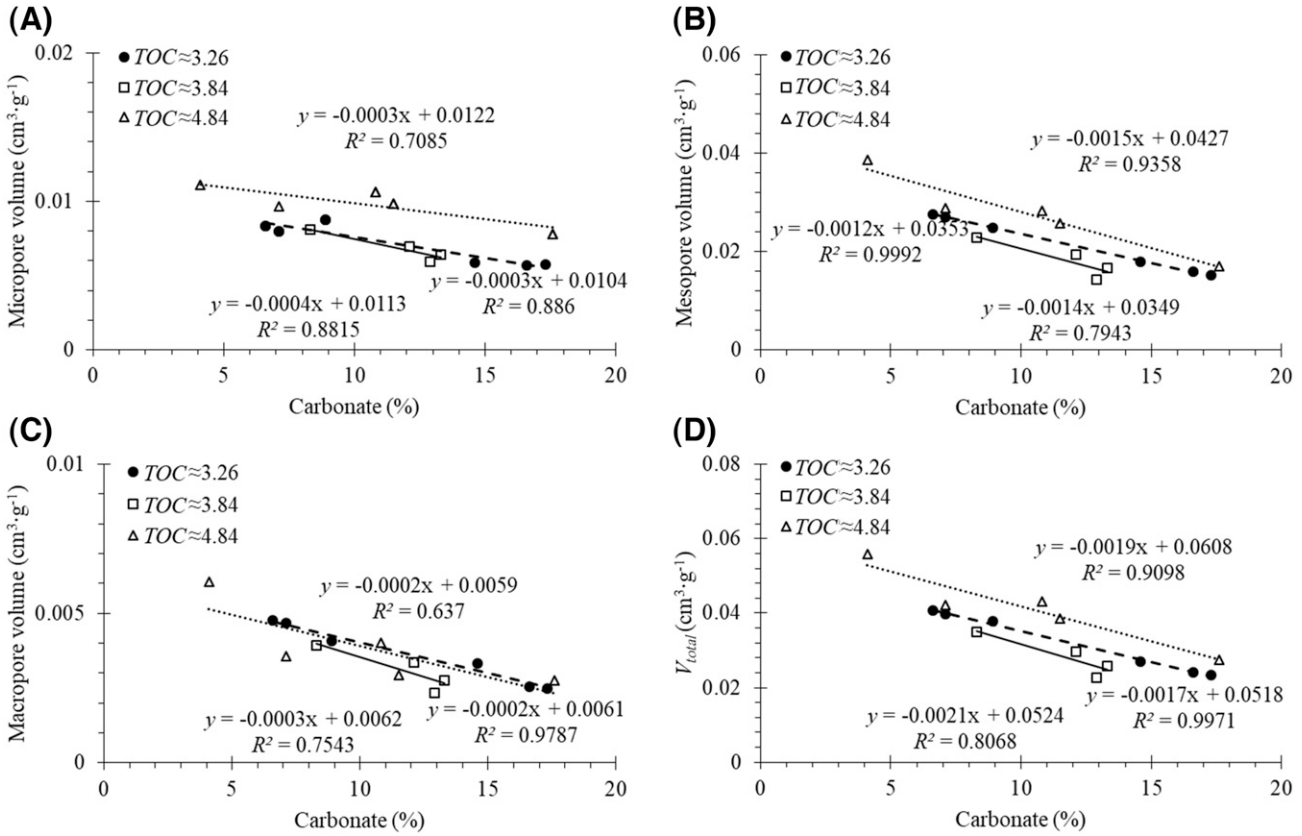

Figure 14. Relationship between the volumes of nanopores and carbonate contents (%) for selected shale samples grouped according to their total organic carbon (*TOC*) contents. (A) Micropore volume (V_{mic}) versus carbonate content; (B) mesopore volume (V_{mes}) versus carbonate content; (C) macropore volume (V_{mac}) versus carbonate content; and (D) total pore volume ($V_{total} = V_{mic} + V_{mes} + V_{mac}$) versus carbonate content. R^2 = coefficient of determination.

their gas contents. Both diagenetic and tectonic factors seem to have played a role in affecting the shale petrophysical properties in the two shale gas fields.

Effect of the Carbonate Cementation on Petrophysical Properties

The FE-SEM imaging studies show that carbonate grains are usually scattered in shales where carbonate content is low (<10%; Schieber, 2010). The presence of scattered carbonate grains does not seem to affect the petrophysical properties of shales (e.g., SH-125a) significantly in this study. A good linear relationship exists between pore volume, specific surface area, and *TOC* content for all of the shale samples with a carbonate content <10% (Figures 5, 6). This is consistent with previous findings by Chalmers et al. (2012), Milliken et al. (2013), Loucks and Reed (2014), and Zhao et al. (2017b). Because the carbonate contents of the Wufeng-Longmaxi shales from the SH-1 well range from 4.1% to 25.9%, three groups of the shale samples with similar *TOC* values but different carbonate contents were selected to further elucidate the specific relationship between the pore volume and carbonate contents.

Figure 14 shows the crossplots of carbonate contents versus volumes of micropores, mesopores, macropores, and total pores obtained from NLDFT adsorption method for the three sets of the shale samples that have three different levels of *TOC* contents and varying contents of carbonate. The volume of all three types of pores is negatively correlated with carbonate contents. The V_{total} values of organic-rich shale samples with similar *TOC* values decrease by ~30%, with a 10% increase in their carbonate contents (i.e., *TOC* ≈ 3.26 wt. %; Figure 14D). This negative correlation between pore volume and carbonate contents also holds for specific surface area versus carbonate contents (Figure 15). Although the slope of the linear regression is slightly different for

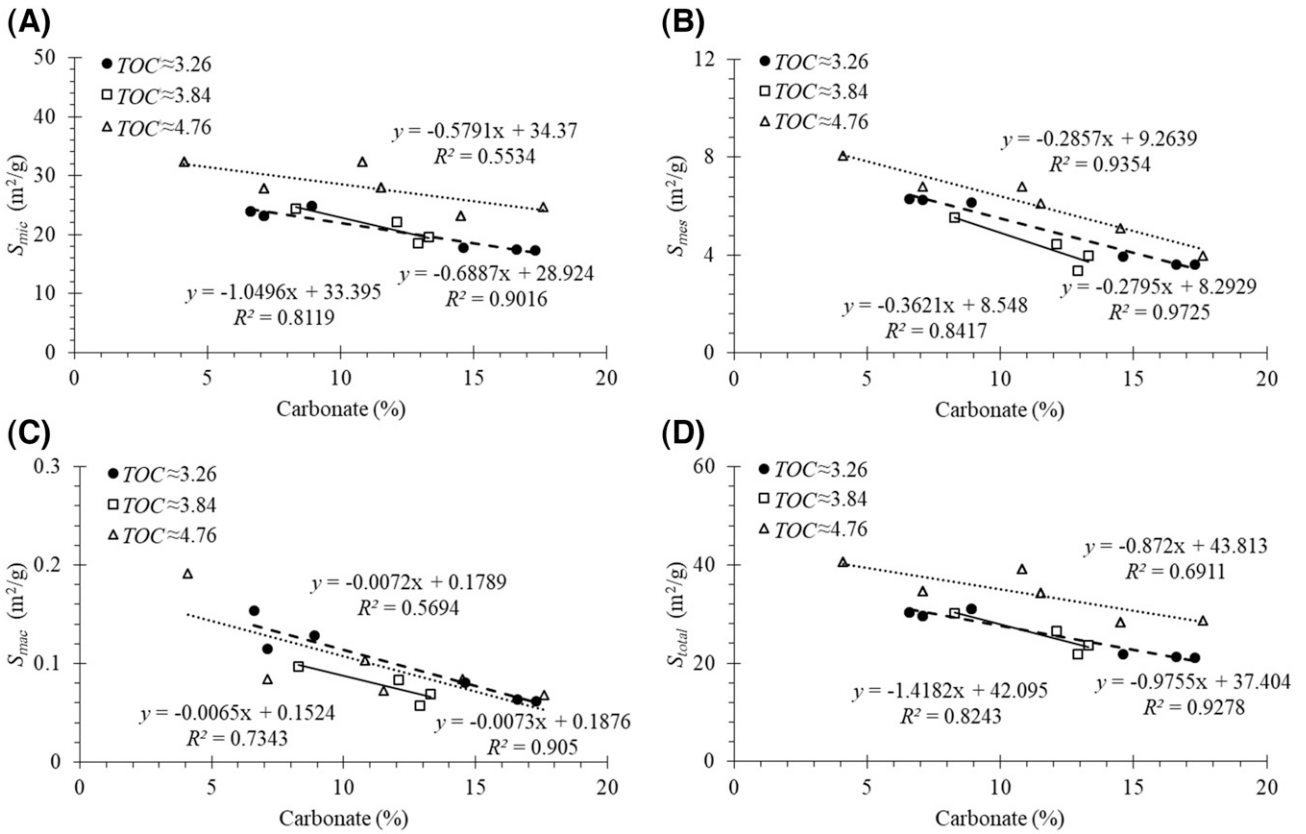

Figure 15. Relationship between the specific surface area of nanopores and carbonate content (%) for selected shale samples grouped according to their total organic carbon (*TOC*) contents. (A) Micropore specific surface area (S_{mic}) versus carbonate content; (B) mesopore specific surface area (S_{mes}) versus carbonate content; (C) macropore specific surface area (S_{mac}) versus carbonate content; and (D) total pore specific surface area ($S_{total} = S_{mic} + S_{mes} + S_{mac}$) versus carbonate content. R^2 = coefficient of determination.

the three *TOC* levels of organic-rich shale samples, higher carbonate content does lead to lower specific surface area. For the sample groups having the best linear relationship between the specific surface area and carbonate contents (i.e., *TOC* ≈ 3.26 wt. %), S_{total} values decrease by approximately 30%, with an increase of 10% in carbonate content (Figure 15D), similar to the above observation on pore volume.

Diagenesis in shales is profound and ubiquitous (Milliken et al., 2012). It is well established that not only oil and gas but also considerable amounts of organic acids and CO_2 can be formed during the thermal evolution of OM (MacGowan and Surdam, 1990; Jarvie et al., 2007; Morad et al., 2010; Schieber, 2010). While the amounts of organic acids and CO_2 generated depends on both the content and type of OM, these substances do not migrate a long distance in organic-rich shale reservoirs with low porosity and permeability (Loucks et al., 2009). As a result, significant amounts of carbonate and feldspar minerals in these shales were dissolved. That many primary interparticle pores in the organic-rich and carbonate-rich shale samples are filled with carbonate cement (Figure 12) is likely due to the occurrence of extensive carbonate dissolution followed by later reprecipitation. Because carbonate minerals are chemically unstable (Schieber, 2010), the pore space among rigid grains such as quartz, the remaining feldspar, and carbonate can be further decreased after or synchronous with mechanical compaction. The unsupported compaction could also retard the development of the organic pore system during the formation of secondary organic pores. This may account for the reduced development of visible organic pores in OM patches close to the calcite (Figure 11B) or isolated from pore networks of shales by carbonate cement (Figure 12A, B) and the line-to-mosaic contacts among carbonate grains (Figure 12A–C, E). This further indicates that organic-rich shales with high carbonate contents are not favorable for the

preservation of primary interparticle pores nor for the development of secondary organic pores. Therefore, the pore volume and specific surface area of the shale samples are significantly influenced by the presence of carbonates, especially when carbonate content is greater than 10% (Figures 4, 7, 8, 14, 15).

In addition to interparticle pores (Figure 12A, E), natural microcracks (Figure 12D) and fractures (Figure 2) can be filled with carbonate cement in shale intervals with high carbonate contents, resulting in further reduced pore volume and connectivity. As such, intense carbonate cementation can lead to not only reduced pore volume and/or space for free gas storage but also decreased surface area for gas adsorption capacity of the Wufeng-Longmaxi shales in the southern Sichuan Basin. This partially explains why the gas content of the Wufeng-Longmaxi shales is lower in Changning field, which has a higher carbonate content, than in Fuling field, which has a lower carbonate content.

Effect of the Tectonic Compaction Deformation on Porosity and Surface Area

Mechanical compaction can lead to rock distortion and abruption. Detachment layers, which are thought to be the final form of layer-parallel shear bands toward a more localized deformation (Lister and Davis, 1989; Mehl et al., 2005), were observed extensively at the base of the Wufeng-Longmaxi succession (Yan et al., 2003; Guo and Zeng, 2015). Zheng et al. (2018) provided details of the pore structures of the detachment layers in the Wufeng Formation and compared the petrophysical properties of the shale samples from the detachment layers with those of normal shale samples. The V_{total} values of the shale samples in the detachment layers were typically 20%–27% higher than those of normal shale samples, whereas the S_{total} values of the shale samples in the detachment layers exhibited no significant changes (Zheng et al., 2018). Similar to the variation of V_{total}, MICP porosities of the shale samples from the detachment layers in both SQ-1 and SH-1 wells are also much higher than those of the normal shale samples (Figure 16).

Mechanical compaction (i.e., rock distortion) occurs commonly in shales and can lead to a decrease in their pore volume (Budd, 2002; Bridge and Demicco, 2008; Loucks et al., 2012; Zhao et al., 2017a).

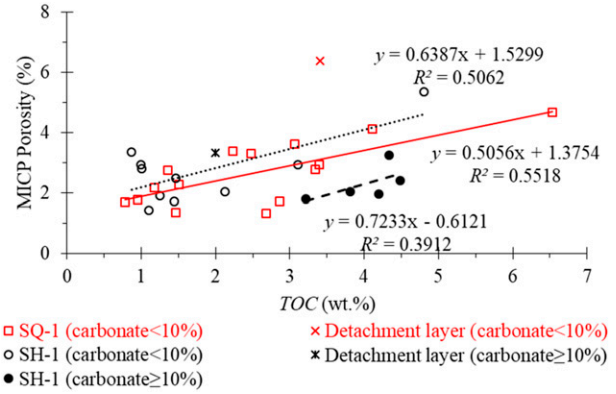

Figure 16. Relationship between porosity measured by mercury injection capillary pressure (MICP) and total organic carbon (*TOC*) contents for the shale samples from Shuanghe-1 (SH-1) and Sanquan-1 (SQ-1) wells. Porosities of samples from the detachment layers in both wells are enhanced compared with those of normal shale samples of similar depth and *TOC* content. R^2 = coefficient of determination.

Pores in shales may be strongly compacted when the external pressure exceeds pore pressure (Handin et al., 1963; Tingay et al., 2009; Liu et al., 2017). Jiao et al. (2018) reported that mechanical compaction can not only reduce pore sizes but also change pore shapes from round or elliptical shaped to slit shaped. Furthermore, mechanical compaction under tectonic stress (i.e., tectonic compaction) may lead to the disappearance of some mesopores (Liang et al., 2017). The effect of tectonic compaction deformation on petrophysical properties is nicely manifested by the V_{total} values of the shale samples with carbonate contents <10% from the three wells in this study. Shale V_{total} values for the SH-1 well that is farther away from the thrust faults are commonly higher than those for both SQ-1 and JY 4 wells that are closer to the thrust faults (Figure 5D). This means that a relatively weak tectonic compaction deformation in Changning ultimately translated into better preservation of pore volume in shale. As a result, the nanopore volume, and hence the space for free gas, in the Wufeng-Longmaxi shales may have been influenced by the tectonic compaction deformation to varying degrees in different parts of the Sichuan Basin.

Despite the above-observed effect of tectonic compaction on total pore volume, neither micropore volume nor micropore specific surface area of the studied shale samples seem to have been affected by

tectonic compaction deformation (Figures 5A, 6A). Because methane adsorption capacity is dominantly controlled by micropore volume and micropore specific surface area (Wang et al., 2016; Zhao et al., 2016a), this observation suggests that the gas adsorption capacity of the Wufeng-Longmaxi shales in the two gas fields has not been significantly affected by tectonic compaction deformation, no matter whether the shale samples are from the detachment layers or not.

Implications for Shale Gas Production

A better understanding of the pore restriction mechanisms and their effects on the shale reservoirs may assist in the identification of favorable shale intervals in a shale gas field. Compared with shale intervals in the eastern Sichuan Basin (e.g., JY 4 and SQ-1 wells), higher carbonate contents (and the associated intensive carbonate cementation) in shales from the southern Sichuan Basin (e.g., SH-1 well) is likely one important geological factor negatively affecting their pore development, gas contents, and ultimately, their shale gas productivity. Due to a relatively weak collision in the southern Sichuan Basin and its neighboring areas, nanopores may have been better preserved in the Wufeng-Longmaxi shales with lower carbonate contents in Changning field. However, the degradation of the Wufeng-Longmaxi shale reservoir property resulting from intensive carbonate cementation dominantly occurs in shale intervals with higher carbonate contents (e.g., SH-1 well). Although the organic-rich shale intervals in Changning and Fuling can be up to 30–50 m (98–164 ft) thick (Zou et al., 2016a), fractures induced by current hydraulic fracturing operations can only reach up to a maximum of 12–13 m (39–44 ft) vertically (Jia et al., 2017). Therefore, the shale interval with both high *TOC* but low carbonate contents in the middle Rhuddanian member of the Longmaxi Formation is likely the best target zone for shale gas drilling and production in the southern Sichuan Basin and its neighboring areas.

CONCLUSIONS

Two shallow wells, SH-1 in Changning field and SQ-1 near Fuling field, were drilled to study how carbonate cementation and tectonic compaction deformation have affected the petrophysical properties of the Wufeng-Longmaxi shales in the southern (e.g., Changning field) and southeastern (e.g., Fuling field) Sichuan Basin. Analytical results on petrophysical properties, OM pore structure, *TOC* contents, bitumen reflectance, and mineralogy of the Wufeng-Longmaxi shales were acquired on both wells together with the JY 4 well from the Fuling field.

Geochemical data indicated similar thickness, *TOC* contents, kerogen type, thermal maturity, and brittle mineral contents for the high-quality Wufeng-Longmaxi shale intervals in both the Changning and Fuling fields. The Wufeng-Longmaxi shales in the Changning field, however, have relatively lower porosities than those from the Fuling field. The results further indicated that pore volume, porosity, and specific surface area of the Wufeng-Longmaxi shales are not only controlled by *TOC* contents but also seem to be significantly affected by carbonate cementation and tectonic compaction deformation. Compared with the Wufeng-Longmaxi shales from Fuling field, the organic-rich shales in the Wufeng Formation and the base of the Longmaxi Formation in Changning field contain much higher contents of carbonate (≥10%, mostly calcite) and commonly have lower pore volume, porosity, and specific surface area. The V_{total} for shale samples with similar *TOC* values can decrease by approximately 30% with an increase of 10% in their carbonate contents. This variation trend also holds for the corresponding S_{total} of the organic-rich shale samples, especially when the carbonate content is in the range of 10% to 20%. Intensive carbonate cementation during diagenesis seems to be a destructive factor that has degraded the petrophysical properties of the Wufeng-Longmaxi shales, and hence the quality of the shale reservoirs. In addition, the relatively weak tectonic compaction deformation in Changing field that is relatively far away from the thrust belts have likely led to better pore preservation compared to Fuling field closer to the thrust belts. Nevertheless, the specific surface area values of the shale samples in different regions do not seem to have been affected by tectonic compaction deformation. Based on the present study, the organic-rich shale intervals with low carbonate contents (and high porosity) in the middle Rhuddanian member of the Longmaxi Formation appear be the optimal target for shale gas

drilling and gas production in the southern Sichuan Basin and its neighboring areas.

REFERENCES CITED

Bernard, S., R. Wirth, A. Schreiber, H. Schulz, and B. Horsfield, 2012, Formation of nanoporous pyrobitumen residues during maturation of the Barnett Shale (Fort Worth Basin): International Journal of Coal Geology, v. 103, no. 23, p. 3–11, doi:10.1016/j.coal.2012.04.010.

Bridge, J. S., and R. V. Demicco, 2008, Earth surface processes, landforms and sediment deposits: New York, Cambridge University Press, 830 p., doi:10.1017/CBO9780511805516.

Budd, D. A., 2002, The relative roles of compaction and early cementation in the destruction of permeability in carbonate grainstones: A case study from the Paleogene of west-central Florida, USA: Journal of Sedimentary Research, v. 72, no. 1, p. 116–128, doi:10.1306/061501720116.

Cao, T. T., Z. G. Song, S. B. Wang, X. X. Cao, Y. Li, and J. Xia, 2015, Characterizing the pore structure in the Silurian and Permian shales of the Sichuan Basin, China: Marine and Petroleum Geology, v. 61, p. 140–150, doi:10.1016/j.marpetgeo.2014.12.007.

Chalmers, G. R. L., R. M. Bustin, and I. M. Power, 2012, Characterization of gas shale pore systems by porosimetry, pycnometry, surface area, and field emission scanning electron microscopy/transmission electron microscopy image analyses: Examples from the Barnett, Woodford, Haynesville, Marcellus, and Doig units: AAPG Bulletin, v. 96, no. 6, p. 1099–1119, doi:10.1306/10171111052.

Chen, L., Y. C. Lu, S. Jiang, J. Q. Li, T. L. Guo, and C. Luo, 2015, Heterogeneity of the Lower Silurian Longmaxi marine shale in the southeast Sichuan Basin of China: Marine and Petroleum Geology, v. 65, p. 232–246, doi:10.1016/j.marpetgeo.2015.04.003.

Choquette, P. W., and L. C. Pray, 1970, Geologic nomenclature and classification of porosity in sedimentary carbonates: AAPG Bulletin, v. 54, no. 2, p. 207–250, doi:10.1306/5D25C98B-16C1-11D7-8645000102C1865D.

Clarkson, C. R., M. Freeman, L. He, M. Agamalian, Y. B. Melnichenko, M. Mastalerz, R. M. Bustin, A. P. Radlinski, and T. P. Blach, 2012, Characterization of tight gas reservoir pore structure using USANS/SANS and gas adsorption analysis: Fuel, v. 95, no. 1, p. 371–385, doi:10.1016/j.fuel.2011.12.010.

Curtis, J. B., 2002, Fractured shale-gas systems: AAPG Bulletin, v. 86, no. 11, p. 1921–1938, doi:10.1306/61EEDDBE-173E-11D7-8645000102C1865D.

Curtis, M. E., B. J. Cardott, C. H. Sondergeld, and C. S. Rai, 2012, Development of organic porosity in the Woodford Shale with increasing thermal maturity: International Journal of Coal Geology, v. 103, p. 26–31, doi:10.1016/j.coal.2012.08.004.

Dutton, S. P., C. D. White, B. J. Willis, and D. Novakovic, 2002, Calcite cement distribution and its effect on fluid flow in a deltaic sandstone, Frontier Formation, Wyoming: AAPG Bulletin, v. 86, no. 12, p. 2007–2021, doi:10.1306/61EEDDE6-173E-11D7-8645000102C1865D.

Guo, T. L., and H. R. Zhang, 2014, Formation and enrichment mode of Jiaoshiba shale gas field, Sichuan Basin: Petroleum Exploration and Development, v. 41, no. 1, p. 31–40, doi:10.1016/S1876-3804(14)60003-3.

Guo, T. L., and P. Zeng, 2015, The structural and preservation conditions for shale gas enrichment and high productivity in the Wufeng–Longmaxi Formation: Southeastern Sichuan Basin: Energy Exploration and Exploitation, v. 33, no. 3, p. 259–276, doi:10.1260/0144-5987.33.3.259.

Guo, X. S., D. F. Hu, Y. P. Li, X. F. Wei, Q. B. Wang, and H. Zhang, 2016, Technologies in discovery and exploration of Fuling Shale Gas Field, China: Natural Resources, v. 7, no. 5, p. 271–286, doi:10.4236/nr.2016.75024.

Guo, X. S., Y. P. Li, R. B. Liu, and Q. B. Wang, 2014, Characteristics and controlling factors of micropore structures of the Longmaxi Shale in the Jiaoshiba area, Sichuan Basin: Natural Gas Industry B, v. 1, no. 2, p. 165–171, doi:10.1016/j.ngib.2014.11.007.

Gutierrez, M., and M. Wangen, 2005, Modeling of compaction and overpressuring in sedimentary basins: Marine and Petroleum Geology, v. 22, no. 3, p. 351–363, doi:10.1016/j.marpetgeo.2005.01.003.

Han, C., Z. X. Jiang, M. Han, M. H. Wu, and W. Lin, 2016, The lithofacies and reservoir characteristics of the Upper Ordovician and Lower Silurian black shale in the Southern Sichuan Basin and its periphery, China: Marine and Petroleum Geology, v. 75, p. 181–191, doi:10.1016/j.marpetgeo.2016.04.014.

Han, Y. J., B. Horsfield, R. Wirth, N. Mahlstedt, and S. Bernard, 2017, Oil retention and porosity evolution in organic-rich shales: AAPG Bulletin, v. 101, no. 6, p. 807–827, doi:10.1306/09221616069.

Handin, J., R. V. Hager Jr., M. Friedman, and J. N. Feather, 1963, Experimental deformation of sedimentary rocks under confining pressure: Pore pressure tests: AAPG Bulletin, v. 47, no. 5, p. 717–755, doi:10.1306/BC743A87-16BE-11D7-8645000102C1865D.

Hao, F., H. Y. Zou, and Y. C. Lu, 2013, Mechanisms of shale gas storage: Implications for shale gas exploration in China: AAPG Bulletin, v. 97, no. 8, p. 1325–1346, doi:10.1306/02141312091.

International Union of Pure and Applied Chemistry, Physical Chemistry Division, Commission on Colloid and Surface Chemistry, Subcommittee on Characterization of Porous Solids, 1994: Recommendations for the characterization of porous solids (technical report): Pure and Applied Chemistry, v. 66, no. 8, p. 1739–1758, doi:10.1351/pac199466081739.

Jarvie, D. M., R. J. Hill, T. E. Ruble, and R. M. Pollastro, 2007, Unconventional shale-gas systems: The Mississippian Barnett Shale of north-central Texas as one model for thermogenic shale-gas assessment: AAPG Bulletin, v. 91, no. 4, p. 475–499, doi:10.1306/12190606068.

Jia, C. Y., A. L. Jia, D. B. He, Y. S. Wei, Y. D. Qi, and J. L. Wang, 2017, Key factors influencing shale gas horizontal well production [in Chinese]: Natural Gas Industry, v.

37, no. 4, p. 80–88, doi:10.3787/j.issn.1000-0976.2017.04.010.

Jiang, Q., C. Q. Zhu, N. S. Qiu, and H. Y. Cao, 2015, Paleoheat flow and thermal evolution of the Lower Cambrian Qiongzhushi shale in the southern Sichuan Basin, SW China: Natural Gas Geoscience, v. 26, no. 8, p. 1563–1570.

Jiao, K., Y. H. Ye, S. G. Liu, B. Ran, B. Deng, Z. W. Li, J. X. Li, Z. Q. Yong, and W. Sun, 2018, Characterization and evolution of nanoporosity in superdeeply buried shales: A case study of the Longmaxi and Qiongzhusi shales from MS well #1, North Sichuan Basin, China: Energy & Fuels, v. 32, no. 1, p. 191–203, doi:10.1021/acs.energyfuels.7b02932.

Kuila, U., and M. Prasad, 2013, Specific surface area and pore-size distribution in clays and shales: Geophysical Prospecting, v. 61, no. 2, p. 341–362, doi:10.1111/1365-2478.12028.

Liang, C., Z. X. Jiang, Y. C. Cao, M. H. Wu, L. Guo, and C. M. Zhang, 2016, Deep-water depositional mechanisms and significance for unconventional hydrocarbon exploration: A case study from the lower Silurian Longmaxi shale in the southeastern Sichuan Basin: AAPG Bulletin, v. 100, no. 5, p. 773–794, doi:10.1306/02031615002.

Liang, M. L., Z. X. Wang, L. Gao, C. L. Li, and H. J. Li, 2017, Evolution of pore structure in gas shale related to structural deformation: Fuel, v. 197, p. 310–319, doi:10.1016/j.fuel.2017.02.035.

Lister, G. S., and G. A. Davis, 1989, The origin of metamorphic core complexes and detachment faults formed during Tertiary continental extension in the northern Colorado River region, U.S.A.: Journal of Structural Geology, v. 11, no. 1–2, p. 65–94, doi:10.1016/0191-8141(89)90036-9.

Liu, Y. K., Y. Q. Xiong, Y. Li, and P. A. Peng, 2017, Effects of oil expulsion and pressure on nanopore development in highly mature shale: Evidence from a pyrolysis study of the Eocene Maoming oil shale, south China: Marine and Petroleum Geology, v. 86, p. 526–536, doi:10.1016/j.marpetgeo.2017.06.012.

Liu, Z. 2018, Fuling shale gas field has proven reserves of 600.8 billion cubic meters, becoming the largest shale gas field in my country, accessed January 1, 2018, https://cq.qq.com/a/20180111/009305.htm.

Loucks, R. G., and R. M. Reed, 2014, Scanning-electron-microscope petrographic evidence for distinguishing organic-matter pores associated with depositional organic matter versus migrated organic matter in mudrocks: GCAGS Journal, v. 3, p. 51–60.

Loucks, R. G., R. M. Reed, S. C. Ruppel, and U. Hammes, 2012, Spectrum of pore types and networks in mudrocks and a descriptive classification for matrix-related mudrock pores: AAPG Bulletin, v. 96, no. 6, p. 1071–1098, doi:10.1306/08171111061.

Loucks, R. G., R. M. Reed, S. C. Ruppel, and D. M. Jarvie, 2009, Morphology, genesis, and distribution of nanometer-scale pores in siliceous mudstones of the Mississippian Barnett Shale: Journal of Sedimentary Research, v. 79, no. 12, p. 848–861, doi:10.2110/jsr.2009.092.

Lucia, F. J., 1995, Rock-fabric/petrophysical classification of carbonate pore space for reservoir characterization: AAPG Bulletin, v. 79, no. 9, p. 1275–1300, doi:10.1306/7834D4A4-1721-11D7-8645000102C1865D.

Luo, Q. Y., N. N. Zhong, N. Dai, and W. Zhang, 2016, Graptolite-derived organic matter in the Wufeng–Longmaxi Formations (Upper Ordovician–Lower Silurian) of southeastern Chongqing, China: Implications for gas shale evaluation: International Journal of Coal Geology, v. 153, p. 87–98, doi:10.1016/j.coal.2015.11.014.

Ma, B. B., Y. C. Cao, K. A. Eriksson, Y. C. Jia, and B. C. Gill, 2017, Depositional and diagenetic controls on deeply-buried Eocene sublacustrine fan reservoirs in the Dongying Depression, Bohai Bay Basin, China: Marine and Petroleum Geology, v. 82, p. 297–317, doi:10.1016/j.marpetgeo.2017.02.014.

Ma, Y., N. N. Zhong, L. J. Cheng, Z. J. Pan, N. Dai, Y. Zhang, and L. Yang, 2016, Pore structure of the graptolite-derived OM in the Longmaxi Shale, southeastern Upper Yangtze Region, China: Marine and Petroleum Geology, v. 72, p. 1–11, doi:10.1016/j.marpetgeo.2016.01.009.

MacGowan, D. B., and R. C. Surdam, 1990, Carboxylic acid anions in formation waters, San Joaquin Basin and Louisiana Gulf Coast, U.S.A.: Implications for clastic diagenesis: Applied Geochemistry, v. 5, no. 5-6, p. 687–701, doi:10.1016/0883-2927(90)90065-D.

Mastalerz, M., A. Schimmelmann, A. Drobniak, and Y. Chen, 2013, Porosity of Devonian and Mississippian New Albany Shale across a maturation gradient: Insights from organic petrology, gas adsorption, and mercury intrusion: AAPG Bulletin, v. 97, no. 10, p. 1621–1643, doi:10.1306/04011312194.

Mehl, C., L. Jolivet, and O. Lacombe, 2005, From ductile to brittle: Evolution and localization of deformation below a crustal detachment (Tinos, Cyclades, Greece): Tectonics, v. 24, no. 4, TC4017, 23 p., doi:10.1029/2004TC001767.

Milliken, K. L., W. L. Esch, R. M. Reed, and T. W. Zhang, 2012, Grain assemblages and strong diagenetic overprinting in siliceous mudrocks, Barnett Shale (Mississippian), Fort Worth Basin, Texas: AAPG Bulletin, v. 96, no. 8, p. 1553–1578, doi:10.1306/12011111129.

Milliken, K. L., M. Rudnicki, D. N. Awwiller, and T. Zhang, 2013, Organic matter hosted pore system, Marcellus formation (Devonian), Pennsylvania: AAPG Bulletin, v. 97, no. 2, p. 177–200, doi:10.1306/07231212048.

Morad, S., K. Al-Ramadan, J. M. Ketzer, and L. F. D. Ros, 2010, The impact of diagenesis on the heterogeneity of sandstone reservoirs: A review of the role of depositional fades and sequence stratigraphy: AAPG Bulletin, v. 94, no. 8, p. 1267–1309, doi:10.1306/04211009178.

Morad, S., J. M. Ketzer, and L. F. D. Ros, 2000, Spatial and temporal distribution of diagenetic alterations in siliciclastic rocks: implications for mass transfer in sedimentary basins: Sedimentology, v. 47, p. 95–120, doi:10.1046/j.1365-3091.2000.00007.x.

Obradors-Prats, J., M. Rouainia, A. C. Aplin, and A. J. Crook, 2017, Assessing the implications of tectonic compaction

on pore pressure using a coupled geomechanical approach: Marine and Petroleum Geology, v. 79, p. 31–43, doi:10.1016/j.marpetgeo.2016.10.017.

Ross, D. J. K., and R. M. Bustin, 2009, The importance of shale composition and pore structure upon gas storage potential of shale gas reservoirs: Marine and Petroleum Geology, v. 26, no. 6, p. 916–927, doi:10.1016/j.marpetgeo.2008.06.004.

Rouquerol, J., and F. Rouquerol, 2014, Adsorption at the liquid–solid interface: Thermodynamics and methodology, *in* J. Rouquerol, F. Rouquerol, K. S. W. Sing, P. Llewellyn, and G. Maurin, eds., Adsorption by powders and porous solids: Principles, methodology and applications, 2nd ed.: New York, Academic Press, p. 105–158, doi:10.1016/B978-0-08-097035-6.00004-8.

Rowley, D. B., 1996, Age of initiation of collision between India and Asia: A review of stratigraphic data: Earth and Planetary Science Letters, v. 145, no. 1-4, p. 1–13, doi:10.1016/S0012-821X(96)00201-4.

Schieber, J., 2010, Common themes in the formation and preservation of porosity in shales and mudstones - Illustrated with examples across the Phanerozoic: Society of Petroleum Engineers Unconventional Gas Conference, Pittsburgh, Pennsylvania, February 23–25, 2010, SPE-132370-MS, 12 p, doi:10.2118/132370-MS.

Schoenherr, J., R. Littke, J. L. Urai, P. A. Kukla, and Z. Rawahi, 2007, Polyphase thermal evolution in the Infra-Cambrian Ara Group (South Oman Salt Basin) as deduced by maturity of solid reservoir bitumen: Organic Geochemistry, v. 38, no. 8, p. 1293–1318, doi:10.1016/j.orggeochem.2007.03.010.

Shen, C. B., L. F. Mei, Z. P. Xu, and J. G. Tang, 2007, Architecture and tectonic evolution of composite basin-mountain system in Sichuan Basin and its adjacent areas [in Chinese]: Geotectonica et Metallogenia, v. 31, no. 3, p. 288–299.

Tang, X. L., Z. X. Jiang, Z. Li, Z. Y. Gao, Y. Q. Bai, S. Zhao, and J. Feng, 2015, The effect of the variation in material composition on the heterogeneous pore structure of high-maturity shale of the Silurian Longmaxi formation in the southeastern Sichuan Basin, China: Journal of Natural Gas Science and Engineering, v. 23, p. 464–473, doi:10.1016/j.jngse.2015.02.031.

Tingay, M. R., R. R. Hillis, R. E. Swarbrick, C. K. Morley, and A. R. Damit, 2009, Origin of overpressure and pore-pressure prediction in the Baram province, Brunei: AAPG Bulletin, v. 93, no. 1, p. 51–74, doi:10.1306/08080808016.

Wang, Y., Y. M. Zhu, S. M. Liu, and R. Zhang, 2016, Pore characterization and its impact on methane adsorption capacity for organic-rich marine shales: Fuel, v. 181, p. 227–237, doi:10.1016/j.fuel.2016.04.082.

Wang, Y. M., D. Z. Dong, X. J. Li, J. L. Huang, S. F. Wang, and W. Wu, 2015, Stratigraphic sequence and sedimentary characteristics of Lower Silurian Longmaxi Formation in Sichuan Basin and its peripheral areas: Natural Gas Industry B, v. 2, no. 2-3, p. 222–232, doi:10.1016/j.ngib.2015.07.014.

Wei, M. M., L. Zhang, Y. Q. Xiong, J. H. Li, and P. A. Peng, 2016, Nanopore structure characterization for organic-rich shale using the non-local-density functional theory by a combination of N_2 and CO_2 adsorption: Microporous and Mesoporous Materials, v. 227, p. 88–94, doi:10.1016/j.micromeso.2016.02.050.

Yan, D. P., M. F. Zhou, H. L. Song, X. W. Wang, and J. Malpas, 2003, Origin and tectonic significance of a Mesozoic multi-layer over-thrust system within the Yangtze Block (South China): Tectonophysics, v. 361, no. 3, p. 239–254, doi:10.1016/S0040-1951(02)00646-7.

Yang, R., S. He, J. Z. Yi, and Q. H. Hu, 2016, Nano-scale pore structure and fractal dimension of organic-rich Wufeng–Longmaxi shale from Jiaoshiba area, Sichuan Basin: Investigations using FE-SEM, gas adsorption and helium pycnometry: Marine and Petroleum Geology, v. 70, p. 27–45, doi:10.1016/j.marpetgeo.2015.11.019.

Zeng, X. L., S. G. Liu, and C. J. Zhang, 2011, Comparison of Silurian Longmaxi Formation shale of Sichuan Basin in China and carboniferous Barnett Formation shale of Fort Worth Basin in United States [in Chinese]: Geological Bulletin of China, v. 30, no. 2–3, p. 372–384.

Zhao, J. H., Z. J. Jin, Z. K. Jin, Q. H. Hu, Z. Q. Hu, W. Du, C. N. Yan, and Y. K. Geng, 2017a, Mineral types and organic matters of the Ordovician-Silurian Wufeng and Longmaxi shale in the Sichuan Basin, China: Implications for pore systems, diagenetic pathways, and reservoir quality in fine-grained sedimentary rocks: Marine and Petroleum Geology, v. 86, p. 655–674, doi:10.1016/j.marpetgeo.2017.06.031.

Zhao, J. H., Z. K. Jin, Z. J. Jin, X. Wen, and Y. K. Geng, 2017b, Origin of authigenic quartz in organic-rich shales of the Wufeng and Longmaxi Formations in the Sichuan Basin, South China: Implications for pore evolution: Journal of Natural Gas Science and Engineering, v. 38, p. 21–38, doi:10.1016/j.jngse.2016.11.037.

Zhao, J. L., H. Xu, D. Z. Tang, J. P. Mathews, S. Li, and S. Tao, 2016a, A comparative evaluation of coal specific surface area by CO_2 and N_2 adsorption and its influence on CH_4 adsorption capacity at different pore sizes: Fuel, v. 183, p. 420–431, doi:10.1016/j.fuel.2016.06.076.

Zhao, W. Z., J. Z. Li, T. Yang, S. F. Wang, and J. L. Huang, 2016b, Geological difference and its significance of marine shale gases in South China: Petroleum Exploration and Development, v. 43, no. 4, p. 547–559, doi:10.1016/S1876-3804(16)30065-9.

Zheng, Y. J., Y. H. Liao, Y. P. Wang, Y. Q. Xiong, and P. A. Peng, 2018, Organic geochemical characteristics, mineralogy, petrophysical properties and shale gas prospects of the Wufeng–Longmaxi shales in Sanquan town of the Nanchuan District, Chongqing: AAPG Bulletin, v. 102, no. 11, p. 2239–2265, doi:10.1306/04241817065.

Zou, C. N., D. Z. Dong, Y. M. Wang, X. J. Li, J. L. Huang, S. F. Wang, Q. Z. Guan, et al., 2016a, Shale gas in China: Characteristics, challenges and prospects (II): Petroleum Exploration and Development, v. 43, no. 2, p. 166–178, doi:10.1016/S1876-3804(16)30022-2.

Zou, C. N., Z. Yang, J. X. Dai, D. Z. Dong, B. M. Zhang, Y. M. Wang, S. H. Deng, et al., 2015, The characteristics and significance of conventional and unconventional Sinian–Silurian gas systems in the Sichuan Basin, central China: Marine and Petroleum Geology, v. 64, p. 386–402, doi:10.1016/j.marpetgeo.2015.03.005.

Zou, C. N., Z. Yang, S. Q. Pan, Y. Y. Chen, S. H. Lin, J. L. Huang, S. T. Wu, et al., 2016b, Shale gas formation and occurrence in China: An overview of the current status and future potential: Acta Geologica Sinica-English Edition, v. 90, no. 4, p. 1249–1283, doi:10.1111/1755-6724.12769.